Global dynamics of a vibro-impacting linear oscillator

G Whiston

GLOBAL DYNAMICS OF A VIBRO-IMPACTING LINEAR OSCILLATOR

G. S. WHISTON

Central Electricity Research Laboratory, Kelvin Avenue, Leatherhead, England

The steady state, vibro-impacting responses of one dimensional, harmonically excited, linear oscillators are studied by using a modern dynamical systems approach allied with numerical simulation. The steady state motions are attracting sets in the system phase space and capture initial conditions in their domains of attraction. Unlike the free, harmonically excited oscillator, the phase space of a vibro-impacting system may be inhabited by many attracting sets. For example, there are sub-harmonic, multi-impact, periodic orbits and chaotic, steady state responses. In order to build a qualitative understanding of vibro-impact response, an attempt is made to build generic topological models of their phase spaces for physically significant parameter ranges. Use is made of the Poincaré section or stroboscopic mapping technique, essentially following an initial impact forwards or backwards in time to subsequent or previous impacts using a computer. The qualitative understanding gained from the analysis and simulations is discussed in an engineering context.

1. INTRODUCTION

This paper is a sequel to an earlier paper [1] which was concerned with the single impact subharmonic periodic response of a harmonically excited, undamped and preloaded one-dimensional linear oscillator. In the latter paper, it was shown that preloaded systems are very similar to unloaded positive clearance systems in many respects and the parallelism is continued here. Whilst the methods used in reference [1] were local in nature, establishing the existence and stability of such periodic responses, a global point of view is adopted in the present paper. An impacting system can be regarded as a recursive system via the map transforming an impact into its successor, essentially strobing the system at each impact event. The flow of the free dynamical system establishes the correspondence between impacts. The map obtained in this way is 1-1 and differentiable (almost everywhere) and the state space comprising of all (positive) impact velocities and impact times (measured via excitation phase) together with the map is an example of a discrete dynamical system. The "diffeomorphism" will be referred to as the Poincaré map—although the nomenclature is usually reserved for the first return map defined in the neighbourhood of closed orbits of differentiable dynamical systems.

The main purpose of a global analysis to try to gain an understanding of the asymptotic or steady state behaviour of vibro-impacting systems. In the case of the response of an unconstrained linear oscillator, the situation is clear cut. For any parameters and for any initial conditions, the system will eventually settle into a steady state harmonic response—provided that a small amount of damping is present. The phase space of this system only ever contains a single attracting orbit—or fixed point in the stroboscopic plane. However, this is certainly not the general case for a vibro-impacting system where the phase space may be inhabited by many attracting motions. Thus if one selects a random initial

condition, one will not in general know the asymptotic response unless one has a knowledge of the domains of attraction of the various co-existing attracting sets. Moreover, as the system parameters in a vibro-impacting system vary, small changes in parameter can lead to gross changes in the phase space structure—attracting sets may appear or disappear or change their stability type. One therefore needs to gain an understanding of the parameters which induce such topological changes or bifurcations. Such knowledge can be of considerable importance in industrial systems which can be modelled in one dimension. For example, loosely supported components in vibrating plant may clash together (usually with allied tangential sliding). The vibro-impacting may cause wear damage, noise or other forms of undesirable effects. Other types of systems, such as impact printers or automobile tappet-operated valve trains, actually rely on periodically forced vibro-impact.

One of the methods usually adopted to try to avoid deleterious vibro-impacting response in loosely supported structures which cannot be rigidly joined is to apply a preload to take up clearances. However, this method cannot be guaranteed to work. To see this, it is useful to consider the example of a two-dimensional dynamical system whose phase portrait on the plane consists of a stable node surrounded by alternately unstable and stable periodic orbits. It follows that for small disturbances, the system will return to rest, but large disturbances will lead to periodic oscillations. If the damping is sufficiently high, the stable and unstable periodic orbits annihilate, leaving the state of rest as the only asymptotic motion. A similar situation pertains to a preloaded vibro-impacting system. If a moderate preload is applied, the state of rest may be only one of many attracting motions in phase space. Small disturbances will lead to transient impacting which is soon quenched by the preload. A larger perturbation might lead to an initial condition in the domain of attraction of an outlying persistent motion and steady state impacting will set in. One needs to be able to predict a preload sufficiently large to destroy all impacting asymptotic motions in the phase space. A method of calculating a sufficiently large preload to destroy (single impact periodic) attractors was suggested in reference [1]. In this case, one of the problems discussed below is "Given that all periodic single impact responses can be destroyed, will the preload also destroy all the more exotic responses?".

Much progress has been made in recent years in the analysis of vibro-impacting response—mainly by S. W. Shaw and his co-workers [2-7]—via the application of the methods of modern dynamical systems theory. This paper is inspired by the success of these analyses and is intended to provide a contribution to the qualitative and quantitative understanding of the vibro-impact response of preloaded systems.

Before launching into a discussion of the global dynamics of vibro-impacting systems, it is necessary to decide which initial conditions lead to impacts. The latter question is investigated in section 2 and this leads to a definition of the Poincaré map of a system with an instantaneous impact event model described by a coefficient of restitution. Such an impact event model is sufficient to describe those systems where the excitation and natural periods are much longer than any expected impact duration. Section 3 is the kernel of the paper and comprises three parts. In the first part there is a very condensed review of dynamical systems theory which provides a global model of "typical" phase space structure. Then some of the analytical considerations of reference [1] are reviewed and extended yielding quantitative information on the phase space structure in the immediate neighbourhood of single impact periodic responses. The global structure is amenable only to numerical simulation and subsequent parts of section 3 describe "typical" phase space structure for two important types of vibro-impacting systems, in the language of modern dynamical systems theory. Positive clearance systems (zero

effective preload) are described first, the discussion being split into separate sections on systems which have either large or small excitation amplitude to clearance ratios. Preloaded systems are then discussed, there being a similar natural division into systems with large or small excitation amplitude to preload ratios. Finally, section 4 is a review of some of the consequences of the previous deliberations for engineering design and for numerical simulation of multi-dimensional vibro-impacting systems. Areas where further research in the field is required are also described.

2. THE POINCARÉ MAP OF A VIBRO-IMPACTING OSCILLATOR

Consider an undamped, linear, one-dimensional oscillator of mass m and stiffness k excited by a harmonic force $f(t) = F_0 \cos(\omega t)$ in conjunction with a constant positive preload N. The system is described by an ordinary non-linear differential equation in the three-dimensional real linear space R^3: $\dot{\gamma} = g \circ \gamma$ where γ is a solution curve $\gamma: R \to R^3$ and g is a vector field on R^3: i.e., a map $g: R^3 \to R^3$. In component form, the non-dimensional equation is

$$\dot{\gamma}_1 = \gamma_2 = g_1(\gamma_1, \gamma_2, \gamma_3), \qquad \dot{\gamma}_2 = -\gamma_1 + \lambda + \beta \cos(z\gamma_3) = g_2(\gamma_1, \gamma_2, \gamma_3),$$
$$\dot{\gamma}_3 = 1 = g_3(\gamma_1, \gamma_2, \gamma_3).$$

The maps γ_i denote the coordinate representatives, $x_i \circ \gamma$ and g_i are the vector components $x_i \circ g$ where x_i are the coordinate maps $R^3 \to R$. γ_1 is the displacement, γ_2 the velocity and γ_3 the non-dimensional time. An overdot denotes differentiation with respect to the phase $\tau = \omega_0 t$ where $\omega_0^2 = k/m$, ω_0 being the oscillator frequency. The other parameters are the frequency ratio $z = \omega/\omega_0$, (it is assumed that $z \neq 1$), the reduced force amplitude $\beta = F_0/k$ and the reduced preload $\lambda = N/k$. The solution $\gamma\mathbf{x}$ from $\mathbf{x} = (x_0, v_0, \tau_0)$ is given by

$$\gamma_1(\tau) = \{x_0 - \lambda - \beta\gamma \cos(z\tau_0)\} \cos(\tau) + \{v_0 + z\beta\gamma \sin(z\tau_0)\} \sin(\tau) + \beta\gamma \cos[z(\tau + \tau_0)] + \lambda,$$

$$\gamma_2(\tau) = -\{x_0 - \lambda - \beta\gamma \cos(z\tau_0)\} \sin(\tau) + \{v_0 + z\beta\gamma \sin(z\tau_0)\} \cos(\tau) - z\beta\gamma \sin[z(\tau + \tau_0)],$$

$$\gamma_3(\tau) = \tau + \tau_0.$$

The parameter γ in these equations is the magnification factor $(1 - z^2)^{-1}$. It is useful to note at this stage that the phase space of the free system can be replaced by the cylinder $R^2 \times S^1$ obtained by identifying time modulo multiples of the period $2\pi/z$ of the excitation. This is possible because the vector field g is periodic in x_3 and corresponds to rolling up the time dimension. The construction is vital to a conventional interpretation of the vibro-impact stroboscopic map.

Suppose that an inelastic stop is situated at $x = c$ and has a coefficient of restitution $r \in]0, 1[$. That is, in the impact systems any point (c, v, τ) with $v > 0$ is to be identified with $(c, -rv, \tau)$ and inversely, (c, v, τ) with $v < 0$ is to be identified with $(c, -v/r, \tau)$. At this point, it is useful to define the following subspaces of R^3: $L_c = \{x \in R^3 \,|\, x_1 \leqslant c\}$; $E_c = \{x \in R^3 \,|\, x_1 = c\}$; $E_c^{\pm} = \{x \in E_c \,|\, x_2 \geqslant 0 \text{ or } x_2 \leqslant 0\}$; $E_c^0 = E_c^+ \cap E_c^-$. The above notation will also refer to the analogous subspaces of $R^2 \times S^1$. Note that E_c is diffeomorphic to the cylinder $R \times S^1$, where R forms the velocity axis, and that E_c^0 is diffeomorphic to the circle S^1. The question arises of describing which points of L_c will eventually impact under the flow of the free dynamical system.

An initial condition $x \in L_c$ is said to lead to an impact if the free trajectory of g from x crosses E_c^+ at some time $\tau \geqslant x_3$ and the impact time is defined as the least time for this event. Let $I_c \subset L_c$ be the set of points which eventually impact and let $N_c = L_c \setminus I_c$. Describe the impact event as a diffeomorphism $P_1: E_c^+ \to E_c^-$, $(c, v, \tau) \to (c, -rv, \tau)$, which is an

initial condition for the free dynamical system. It is not obvious that this initial condition lies in I_c. This point will be dealt with later. If $x \in L_c$, it is possible that the free trajectory will enter E_c^0: i.e., cross E_c with $v = 0$. If this happens, the global trajectory has a local extremum in x_1 and the nature of the extremum is determined by the sign of the acceleration $\dot{x}_2$. If $\dot{x}_2 = 0$, the degenerate impact is a point of inflection. Because the trajectory is assumed to have an initial condition in L_c, $\dot{x}_2$ is about to go positive and the impact system trajectory must remain in E_c^0 for some time interval. If $\dot{x}_2 < 0$, the degenerate impact is a local maximum and the global trajectory will immediately re-enter L_c. Finally if $\dot{x}_2 > 0$, the degenerate impact is a local minimum of the global trajectory and the trajectory must have crossed E_c^+ at some earlier time. These considerations are summarized in Figure 1. Only degenerate impacts of types (a) and (b) as shown in Figure 1 are of interest. Type (a) degenerate impacts lead to trapping whilst those of type (b) are not trapping. It follows that trapping is a rare event in the sense that it occurs only at the simultaneous zeros of x_2 and $\dot{x}_2$. If it does occur, it is necessary to assume that the impact system trajectory remains in E_c^0 until the acceleration next passes through zero and then use this time in the new initial condition for a free trajectory into L_c. This topic will be covered later. The following proposition is fundamental to establishing the possibility of an infinitely iterable recursive vibro-impact map.

Proposition (1). $E_c^- \cap N$ is empty—all initial conditions (c, v, τ) with $v < 0$ lead to impacts.

Proof. Assume first that z is rational, that is, there exist positive relatively prime integers n and m with $z = n/m$. Then the free trajectory from (c, v, τ) is periodic with period $2\pi m$ and is subharmonic of order n. Because $v < 0$, it follows that the free trajectory crosses E_c^- from $x > c$ and must therefore have crossed E_c^+ in the past. Periodicity then establishes that the trajectory will cross E_c^+ in the future. If z is irrational, the above argument cannot be applied directly since any free trajectory is aperiodic. However, it may be approximated by long period orbits to any accuracy. That is, there exists a sequence of rational numbers $\langle q_k \rangle k \geq 0$ which converges to z and the corresponding periodic orbits lead to a sequence $\langle x_k \rangle k \geq 0$ of finite velocity impacts. Finite velocity implies that there is a compact subspace X of E_c^+ with $x_k \in X$ for each k. But this implies that the sequence $\langle x_k \rangle$ has a limit x in X and therefore in E_c^+. It follows that the free trajectory with irrational z leads to an impact.

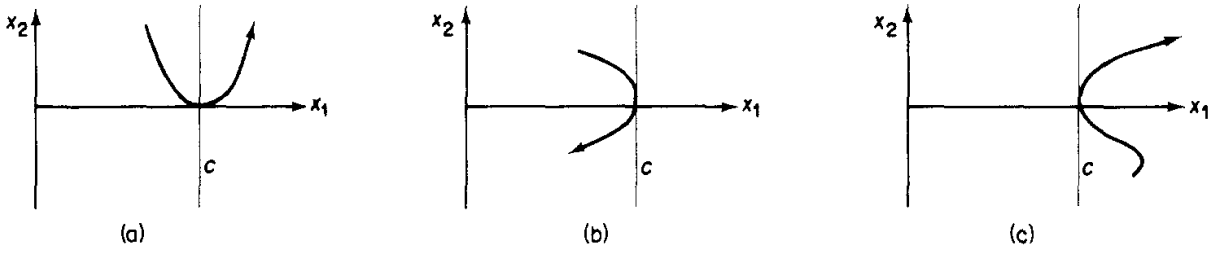

Figure 1. Degenerate impacts. (a) Point of inflection, $\dot{x} = 0$; (b) local maximum, $\dot{x}_2 < 0$; (c) local minimum, $\dot{x}_2 > 0$.

This allows one to define an important map, P_2, from $\mathring{E}_c^-$ into E_c^+; P_2 sends (c, v, τ) with $v < 0$ into (c, u, τ_1) which is the first crossing of E_c^+ by the free trajectory $\gamma \mathbf{x}$ of E_c^+. P_2 cannot be extended over E_c^0 to E_c^-, that is, to zero velocity impacts, without paying a considerable penalty—lack of injectivity. This would mean that a first return map would be uninvertible. The difficulty is due to the possibility of trapping. Given $x \in E_c^0$ at a time τ with positive acceleration, the vibro-impact convention is that the orbit remain in E_c^0 until, if ever, the acceleration passes through zero and each trapped degenerate impact has the same subsequent impact: that is, if τ_0 is the next zero crossing time of the

acceleration, $P_2(c, 0, \tau) = P_2(c, 0, \tau_0)$ for all trapped τ. In this case P_2 would be non-injective. Worse, if τ_0 does not exist, the acceleration on E_c^0 is positive for all τ, P_2 would be undefined—there can be no successive impact for any degenerate impact in this case. Thus although P_2 cannot always be extended to E_c^-, the following paragraphs present a maximal injective extension.

Because of difficulties with degenerate impacts, split E_c^0 into three subspaces, $E_c^0 = A^+ \cup A^0 \cup A^-$ where the acceleration $a(\tau) = \lambda - c + \beta \cos(z\tau)$ is respectively positive, zero or negative. The subspace of E_c^- leading to degenerate impacts can be decomposed in exactly the same way: $P_2^{-1}(E_c^0) = P_2^{-1}(A^+) \cup P_2^{-1}(A^0) \cup P_2^{-1}(A^-)$. These subspaces can be considered in turn. Firstly, $P_2^{-1}(A^+)$ is the empty set—no negative initial velocity on E_c can lead to a degenerate trapped impact. To see this, note that if $x \in P_2^{-1}(A^+)$ then $P_2(x) = (c, 0, \tau_1)$ where $a(\tau_1) > 0$. But then $x_1(\tau_1) = c$ is a local minimum for $x_1(\tau)$ which must imply that $x_1(\tau)$ crosses $x_1 = c$ for some $\tau_0 < \tau_1$—this is impossible because τ_1 is the first crossing time. The following proposition covers the remaining possibilities; either $P_2(x)$ is grazing, $a(\tau_1) < 0$ or $P_2(x)$ is a point of inflection for $x_1(\tau)$. An inflection point is defined as an α point if $\dot{a}(\tau_1) > 0$ or as an ω-point if $\dot{a}(\tau_1) < 0$. Impacts are trapped at an α point and released at an ω-point.

Proposition (2). (1) *Preload systems* ($\lambda > 0$, $c = 0$). If $0 < \lambda < \beta$, A^- is an open interval $]\pi/z - \tau_0, \pi/z + \tau_0[$ about π/z where $0 < \tau_0 < \pi/z$ and τ_0 approaches π/z as λ approaches β; $A_0 = \{\pi/z - \tau_0, \pi/z + \tau_0\}$ and $\pi/z - \tau_0$ is an α point, $\pi/z + \tau_0$ an ω point. If $\lambda = \beta$, A^- is empty and $A^0 = \{\pi/z\}$ is both an α and an ω point. If $\lambda > \beta$, A^- and A^0 are empty. (2) *Clearance systems* ($c \geq 0$, $\lambda = 0$). If $0 \leq c < \beta$, A^- is an interval $]\pi/z - \tau_0, \pi/z + \tau_0[$ about π/z and τ_0 increases monotonically from $\pi/2z$ to π/z as c varies from 0 towards β; $A^0 = \{\pi/z - \tau_0, \pi/z + \tau_0\}$ and $\pi/z + \tau_0$ is an α-point, $\pi/z - \tau_0$ an ω-point. If $c = \beta$, $A^- =]0, 2\pi[$ and $A^0 = \{0\}$ is both an α and an ω-point. For $c > \beta$, $A^- = E_c^0$ and A^0 is empty.

$P_2^{-1}(A^-)$ is the subspace of initial conditions in $\mathring{E}_c^-$ which flow into grazing impact. These present no problems to extending P_2 into E_c^- because a grazing impact either always leads to other grazing impacts, to a subsequent α-point or to a impact event in E_c^+.

In the light of these considerations, one is led to make the following maximal injective extensions of P_2: (1) $\Sigma_c^- \equiv E_c^- \backslash A^+$ if there are α and ω points in E_c^0; if $x \in A^-$ or $x = \omega$, $P_2(x) =$ succeeding impact, and $P_2(\alpha) = \omega$; (2) $\Sigma_c^- = E_c^-$ in a clearance system with either $A^- = E_c^0$ or if a simultaneous α and ω-point exists; then $P_2(x) =$ succeeding impact if $x \in A^-$ or $x = \alpha$; (3) $\Sigma_c^- = \mathring{E}_c^-$ in a preload system with A^- empty when $P_2(\mathring{E}_c^-) \subset \mathring{E}_c^+$.

The map $P_2 : \Sigma_c^- \to \Sigma_c^+$ is 1-1 and differentiable almost everywhere. In cases (2) and (3), P_2 is globally differentiable.

To complete the construction, one has to define Σ_c^+ analogously. Thus in cases (1)-(3) respectively, define $\Sigma_c^+ = E_c^+ \backslash A^+$, E_c^+ or $\mathring{E}_c^+$. The map $P_1 : E_c^+ \to E_c^-$ restricts to $\Sigma_c^+ \to E_c^-$ defining a map $\Sigma_c^+ \to \Sigma_c^-$ which leaves $A^- \cup A^0$ invariant, mapping $\mathring{E}_c^+$ into $\mathring{E}_c^-$ for non-zero coefficient of restitution. To close the systems one now defines the Poincaré map $P : \Sigma_c^+ \to \Sigma_c^+$ by composition of maps, $P = P_2 \circ P_1$ to obtain a globally 1-1 map.

Although large preload systems are conveniently described in the present format, it is useful to visualize an allied non-differentiable but 1-1 Poincaré map defined by shrinking E_c^0 to a point, Ω, say, in a type (3) system and extending P by writing $P'(x) = P(x)$ if $x \neq \Omega$, $P'(\Omega) = \Omega$. The point Ω then acts as a terminal attractor, trajectories of P' disappear through this "black hole" singularity. A similar construction for clearance systems with terminal grazing orbits is conceptually useful. Figure 2 summarizes these constructions in the various cases.

Note that for the clearance terminal systems, Ω represents a graze-only, free orbit. Such an orbit is not stable to small perturbations such as damping, the addition of which

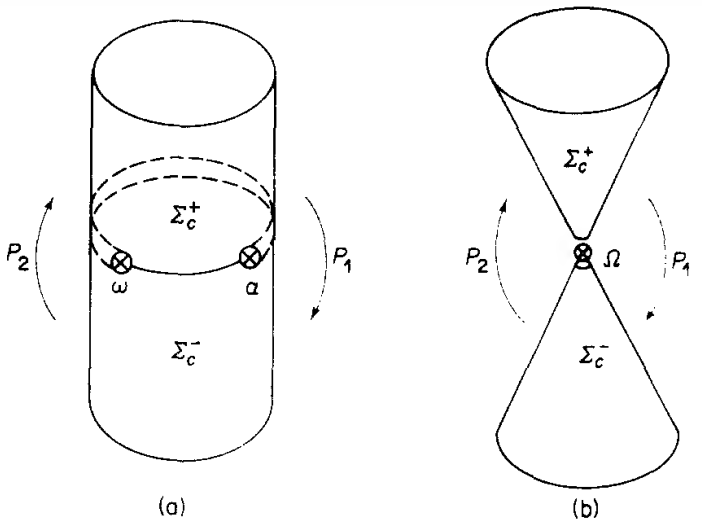

Figure 2. Singular manifolds of vibro-impacting systems. (a) State space for trapping systems; (b) state space for terminal systems.

would replace Ω by the attractive free response orbit. However, one can use either interpretation. The preload static terminal state is robust to such perturbations.

To summarize this section, a Poincaré map $P: \Sigma_c^+ \to \Sigma_c^+$ has been constructed for clearance and pre-load vibro-impact systems. The map may be non-differentiable on a nowhere dense subspace. For example, discontinuities occur on $P^{-1}(Z_c)$, where Z_c denotes the allowable zero velocity impacts in $[\omega, \alpha]$. Non-differentiability plays an important dynamical role and is discussed in detail in reference [17]. In any case, P is injective and will have an inverse allowing one to predict both the past and future history of an impact event.

3. DYNAMICS OF VIBRO-IMPACTING

3.1. GLOBAL DYNAMICS

The mapping $P: \Sigma_c^+ \to \Sigma_c^+$ constructed in section 2 is an example of a (singular) discrete dynamical system. The temporal evolution of an impact event $\mathbf{x} \in \Sigma_c^+$ is described by the orbit of x under all forwards or backwards iterations under P, the totality of orbits comprising the phase portrait of the dynamical system. In general, one is usually only interested in persistent or steady state motions, not in transient motion. Thus one's main interest lies in the asymptotic behaviour of the orbits, usually under forwards iteration, requiring answers to questions such as "where do orbits end up?". The places where orbits end up are called asymptotic limit sets and the following paragraphs comprise a very condensed description of asymptotic limit sets for a widely studied type of discrete dynamical system. It is hoped that the short review will provide background for the ensuing discussion of vibro-impacting systems. The reader is referred to references [8–14] for further details.

Suppose that $f: X \to X$ is a discrete dynamical system on a (compact) differentiable manifold X. Denote the orbit of a point x of X under f by $f[x]$. The question as to where $f[x]$ ends up can be formulated more precisely by seeking those points of X around which the orbit accumulates. Define partial orbits $f_+^k[x] \equiv \{f^m(x) \,|\, m \geq k\}$ where $k \geq 0$ is an integer. Evolution along the orbit is described by the diminishing sequence of sub-orbits: $\cdots \subset f_+^{k+1}[x] \subset f_+^k[x] \cdots \subset f_+^0[x]$. The sequence of closures of the sub-orbits forms a similar apparently decreasing sequence and the latter sequence "converges" to the ω-limit set of x: $\omega(x) = \bigcap_{k \geq 0} \mathrm{Cl}\,(f_+^k[x])$. A point y lies in $\omega(x)$ if and only if there is a sequence of points descending the orbit of x which converges to y. Thus the orbit

of x asymptotically "wraps" itself around $\omega(x)$ as indeed must the orbit of any other point in $f[x]$. A similar construction involving f^{-1} defines $\alpha(x)$, the α-limit set of (the orbit of) x, describing the "origin" of the orbit. The collection of all $\omega(x)$ plus all $\alpha(x)$ is called the asymptotic limit set $L(f)$ of the dynamical system and describes all the periodic and recurrent behaviour. There is a class of dynamical systems where the set $L(f)$ is particularly well understood—those where $L(f)$ is hyperbolic. In this case, one can apply the spectral decomposition theorem. $L(f)$ can be split into a finite sum of closed disjoint f-invariant sets L_k each of which contains a dense orbit and has periodic points dense. The decomposition arises from the result that if $L(f)$ is hyperbolic, then the set of all periodic points of f, $Per(f)$, is dense in $L(f)$. The set $Per(f)$ can be partitioned into disjoint equivalence classes under the relationship of h-equivalence, two periodic points being called h-equivalent if there exist reciprocal transversal intersections of their stable and unstable manifolds. The closures of the h-classes provide the partition of $L(f)$. Moreover, the dynamics of f on each basic limit set L_k can be described particularly neatly via the methods of symbolic dynamics. The hyperbolic structure of $L(f)$ allows one to define the stable manifolds of the basic limit sets as points which converge to one of the limit sets under forwards iteration and it follows that X can itself be decomposed into a sum of "domains of attraction" of the basic limit sets. $L(f)$ is a subset of the non-wandering set $\Omega(f)$ of f and a dynamical system is called "axiom A" if $\Omega(f)$ is hyperbolic and $Per(f)$ is dense in $\Omega(f)$. For such systems, $\Omega(f)$ has a directly similar spectral composition, but one can also define an order relation between the basic sets by writing $\Omega_k < \Omega_j$ if $W^s(\Omega_k) \cap W^u(\Omega_j)$ is non-empty: that is, there is an orbit from Ω_j to Ω_k. Basic sets lying at the ends of the order branches are attractors and correspond to stable nodes; all others correspond to saddles. One therefore gains a fairly detailed model of the phase space structure of axiom A systems. In particular, X decomposes into a set of domains of attraction of a finite number of invariant limit sets which have a good description in terms of symbolic dynamics.

In two dimensions, one can begin to describe hyperbolic attractors in some detail. For example, if Λ is a hyperbolic attractor in a two dimensional dynamical system, it must be a stable node or have topological dimension 1. In the latter case, Λ coincides with the closure of the union of the unstable manifolds of its points each of which is an immersed 1-manifold. An excellent description of one-dimensional hyperbolic attractors is to be found via the theory of expanding maps on branched 1-manifolds based upon Smale's classic solenoidal expanding attractor. The latter example connects rather nicely with fractal microstructure in such attractors in that there is a rather direct representation of the attractor as a Cantor 1-manifold, locally $R \times C$ where C is the classic Cantor set of excluded middles of the unit interval. One therefore gains an instructive picture of Λ as a complex collection of arbitrarily close linear segments packed into a compact subspace of X. There may be infinitely many points with dense orbits and the orbits of these points expand eternally inside Λ which may also contain infinitely many periodic points of any period. A particularly interesting example of a repelling basic set which is highly relevant to the present study occurs in systems have undergone a homoclinic bifurcation. In this case, as a parameter varies, components of the stable and unstable manifolds of a saddle point pass from tangential intersection through to transversal intersection. Tangential and transversal intersections must occur at an infinite number of points. In the case of transversal intersection, the λ-lemma implies that W^u accumulates along itself and W^s accumulates along itself in a rapidly oscillating fashion as depicted in Figure 3 for dimension 2. In this case, the homoclinic tangle acts as a repelling set although it contains an infinite number of invariant sets of incredible complexity. Indeed, the Smale homoclinic theorem states that if $W^s(p)$ and $W^u(p)$ intersect transversally at $x \neq p$ there exists a

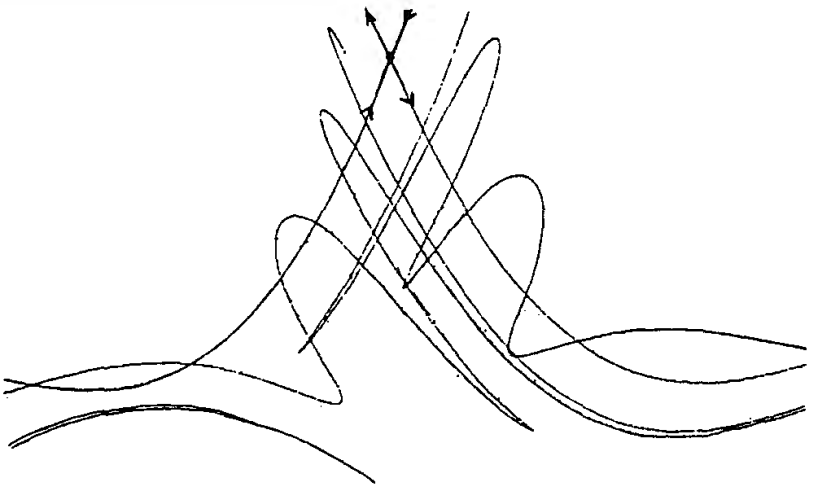

Figure 3. Part of a homoclinic tangle observed in a vibro-impact system. The state space is a cylinder.

hyperbolic invariant set Λ containing x and p such that for some n, f^n is C^0 equivalent to a shift on two symbols.

Examples of all the above types of complicated structures occur very frequently in vibro-impacting systems. The parallel with the well understood axiom A systems is not yet clear. For example, Σ_c^+ is non-compact and sometimes singular. Non-compactions is not a problem in that one can always replace Σ_c^+ by an appropriate compactification although it is not clear what role the singularity structure plays. However, in all the simulations so far observed, a finite number of indecomposable limit sets has been observed and the local structure of the attracting sets seems to have the necessary local expansion/contraction required for hyperbolicity. Clearly, further work is required.

One can demonstrate the existence of attracting sets in vibro-impact systems using elementary energy balance arguments. The same argument together with non-compactness of Σ_c^+ also demonstrates that $\alpha(P)$, the α-limit set of P, is empty. An attracting set can be described as an f-invariant subset A with an open neighbourhood U such that points of U flow into A. Equivalently, $A = \bigcap_{k \geq 0} f^k(U)$. Given an open f-invariant set U, there is an allied attracting set $U_\infty = \bigcap_{k \geq 0} f^k(U)$ which may be empty and need not be indecomposable. It follows that the existence of an f-invariant open set sometimes implies the existence of attracting sets around which U is ultimately wrapped by f. In an inelastic vibro-impacting system, the energy loss per impact at velocity v is $mv^2(1-r^2)/2$. During the subsequent rebound, the excitation supplies energy. Suppose that the first impact occurs at time t_0 followed at time t_1 by a second. Then the energy gain is

$$\int_{t_0}^{t_1} F_0 \cos(\omega t)\{(-A \sin[\omega_0(t-t_0)] + B \cos[\omega_0(t-t_0)])\omega_0 + \omega\gamma_0 \cos(\omega t)\}\, dt$$

where $\gamma_0 = (\omega^2 - \omega_0^2)^{-1}$, $A = [c - \gamma_0 F_0 \cos(\omega t_0)]$ and $B = [v + \omega\gamma_0 F_0 \sin(\omega t_0)]$. It therefore follows that the energy gain is linear in v, $\alpha(t_0, t_1)v + \beta(t_0, t_1)$, whilst the energy loss is quadratic. For large enough impact velocities, the subsequent impact will be at lower velocity and it follows that there exists an open subspace U of Σ_c^+ such that $P(U) \subset U$, implying that U_∞ is an attracting set. U is of the form $[0, \gamma_*]xS^1$ and it follows that the α-limit set, $\alpha(P)$, is empty; all orbits entering U come from infinity. (In a preload system, U_∞ may be empty.)

3.2. LOCAL DYNAMICS

Before launching into a discussion of the global dynamics of vibro-impacting, the following paragraphs present a review of the local dynamics in the neighbourhoods of

fixed points of the Poincaré map representing single impact subharmonic periodic motions. These responses are the only vibro-impact orbits about which one can gain quantitative information on existence and stability [1, 2, 15]. In reference [1], the following quadratic equation for the impact velocity V_n for a period n subharmonic response was obtained:

$$V_n^2(s_n^2(1-r)^2+z^2c_n^2(1+r)^2)+4x_0z^2c_ns_n(1+r)V_n+4z^2s_n^2(x_0^2-\beta^2\gamma^2)=0.$$

Here s_n and c_n denote $\sin(\pi n/z)$ and $\cos(\pi n/z)$. The impact phase of the excitation τ_n of this motion is given by

$$\tan(z\tau_n)=s_n(1-r)V_n/[2zs_nx_0-z(1+r)V_nc_n].$$

The equation applies to both clearance ($\lambda=0$, $c\geq 0$) and preload ($\lambda>0$, $c=0$) systems when x_0 is replaced by c or by $-\lambda$ respectively. Because the defining equation is quadratic, there are two roots, $V_{n\pm}$ at each parameter point with two corresponding impact phases, $\tau_{n\pm}=\tau_n(V_{n\pm})$. The phases $\tau_{n\pm}+\pi/z$ are also solutions since $z\tau_n$ is only defined modulo π by the second of the two preceding equations. It is important to note that the equations were derived by applying the cyclic boundary conditions $(c, -rV_n, \tau_n)$, $(c, V_n, \tau_n+2\pi n/z)$ to the free response solutions without requiring that the free orbit remain within L_c for $\tau\in]\tau_n, \tau_n+2\pi n/z[$. That is, the real positive solutions of the quadratic equation may represent re-entrant free orbits which cross E_c^0 an even number of times within the above time interval. Re-entrancy can only be established numerically and thus a solution was regarded as physical if it was real, positive and finite. In reference [1], the existence of such solutions as a function of frequency ratio z and of $\sigma=x_0/\beta$ was analyzed algebraically. It turned out that, in general, the regions of z parameter space in which physical solutions existed were disjoint intervals near the rational points $2n/m$ for $m\geq 1$. Numerical simulations show that the formal solutions are usually non re-entrant only near $z=2n$, but this is not an absolute rule in that it is possible (although rare) for several distinct subharmonic stable solutions to co-exist. The reader is referred to reference [1] for further details on the complicated physical ranges of frequency ratio. The behaviour of the solutions with σ (clearance or preload: amplitude ratio) is more interesting. There is a critical ratio σ_* when the discriminant of the quadratic equation vanishes

$$\sigma_*=|\gamma|\{1+z^2\cot^2(\pi n/z)[(1+r)/(1-r)]^2\}^{1/2}.$$

Note that, by definition, for $\sigma=\sigma_*$, both roots $V_{n\pm}$ coincide as must the phases $\tau_{n\pm}$. For $\sigma>\sigma_*$, $V_{n\pm}$ are both complex and thus unphysical. For suitable frequency ratio, V_{n+} and V_{n-} are positive for σ just below σ_* and in this case, both roots are physical in the range $]|\gamma|, \sigma_*[$, the lower root, V_{n-}, vanishing at the zero, $\sigma=|\gamma|$ of the constant term of the quadratic. The upper root, V_{n+}, remains positive until $\sigma=-|\gamma|$. It follows that, modulo re-entrancy, two fixed points coexist in $]|\gamma|, \sigma_*[$, a single fixed point can exist in $]-|\gamma|, |\gamma|[$ and that (V_{n+}, τ_{n+}) disappears at $\sigma=-|\gamma|$, (V_{n-}, τ_{n-}) disappears at $\sigma=|\gamma|$ and both (V_{n+}, τ_{n+}) and (V_{n-}, τ_{n-}) simultaneously disappear at coincidence at $\sigma=\sigma_*$. These points must represent bifurcation points of the system. Figure 4 is a schematic stability plot for a clearance system when $\sigma=c/\beta=kc/F_0$.

The stability of the fixed point is determined by the local linearization TP of the Poincaré map, the Jacobian of which is given by

$$\begin{bmatrix} -r(VC_n-NS_n)/V & [(N^2-r^2V^2)S_n-(1-r)VNC_n]/V \\ rS_n/V & (-rVC_n+NS_n)/V \end{bmatrix},$$

where $N=(\beta\cos(z\tau)-x_0)$ and C_n, S_n denote $\cos(2\pi n/z)$ and $\sin(2\pi n/z)$. The eigenvalues $\lambda_\pm$ of TP are expressible as $(T\pm(T^2-4D)^{1/2})/2$ where T denotes the trace and

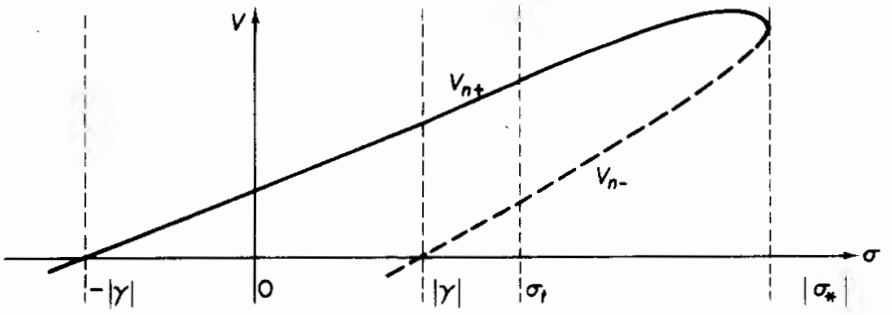

Figure 4. Stability diagram of a clearance system.

D the determinant of TP, the latter quantity being given by $D = r^2$. Because $\lambda_+\lambda_- = D = r^2 < 1$, it follows that unstable nodes cannot exist in a vibro-impact system, for then $\lambda_+ > 1$ and $\lambda_- > 1$. Equivalently, only stable nodes, $\lambda_+ < 1$ and $\lambda_- < 1$, or saddle points, $\lambda_+ > 1$, $\lambda_- = r^2/\lambda_+ < 1$, are allowed hyperbolic fixed points.

For $T^2 > 4D$, both eigenvalues, $\lambda_\pm$ are real whilst for $T^2 \leqslant 4D$, they are both complex which implies that the associated fixed point is a spiral sink with $\lambda_\pm = r \exp(\pm i\theta)$ where $\tan(\theta) = (4D - T^2)^{1/2}/T$ and $|\lambda_\pm| = r < 1$. The coincident point, $\sigma = \sigma_*$, is a point of local bifurcation where one of the eigenvalues attains the value $+1$, the simultaneous disappearance of the fixed points corresponding to V_{n+} and V_{n-} involving a saddle-node bifurcation. Numerical simulations establish that for σ in the internal $]|\gamma|, \sigma_*[$, the points (V_{n+}, τ_{n+}) and (V_{n-}, τ_{n-}) are respectively a spiral sink and a saddle point. Simulations also indicate the existence of further bifurcations in the interval $]-|\gamma|, \sigma_*[$. As σ decreases from σ_* towards $|\gamma|$, there is a homoclinic global bifurcation at $\sigma = \sigma_t$ where there are tangential intersections of the stable and unstable manifolds of the saddle point. Further decreases of σ lead to transversal intersections and the generation of a homoclinic tangle. The bifurcation has the effect of changing the stable node into an "almost global" attractor which captures almost all orbits, excepting those involved with the strange invariant sets associated with the tangle and predicted by the Smale homoclinic theorem. As σ decreases further, there are complex changes in the Birkhoff-Abraham signature of the tangle.

One could now repeat the above discussion of clearance systems for preload systems. All would proceed exactly in parallel but only in a frequency range where the linear term of the quadratic is negative overall for $\sigma = -\lambda/\beta$ negative. The only difference to be noted at this point is that the saddle appears to the left of the sink in the interval $|\sigma| \in]|\gamma|, \sigma_*[$ whereas the opposite holds for clearance systems. Figure 4 is re-obtained except that the σ axis is reversed.

Saddle-node and flip bifurcations were mentioned above. These are the only ones permitted in a vibro-impacting system. Firstly, note that Hopf bifurcations are ruled out by their violating the condition $\det(TP) = r^2 < 1$ in an inelastic system because they require two eigenvalues of unit modulus. The transcritical and pitchfork bifurcations amongst the saddle-node family are also not permitted because they can occur only in systems with high symmetry.

3.3. NUMERICAL SIMULATION

As mentioned in section 3.1, it is possible to apply analytical methods only to local dynamics and therefore one has to resort to numerical methods to obtain a global overview of vibro-impacting. This sub-section presents a brief description of the computer methods used in the simulations described below.

Given a point $x \in \Sigma_c^+$, the point $P(x)$ is defined as the point of Σ_c^+ first crossed by the free response trajectory from the initial condition $P_1(x) \in \Sigma_c^-$. The free response solutions are, of course, known analytically and may be time-stepped from $P_1(x)$ until a crossing

of $x = c$ is detected. Having isolated the crossing point, which is guaranteed to be the first crossing if a sufficiently small time step is used, one can accurately locate the time by bisection or by the Newton–Raphson method (the former being used in the present investigation). The time τ of crossing yields the image point $P(\mathbf{x}) = (\tau, \dot{x}(\tau))$. Some of the maps discussed below were produced by using a 16-bit microcomputer and some by using an IBM 4381. In practice, rather than compute the orbits of arbitrary points, fixed points were usually sought. The maps were drawn in real time, initially iterating from "high" impact velocity, knowing that any attracting sets inhabit "low" velocity regions of Σ_c^+. A trial initial condition was selected and the orbit followed down the cylindrical phase space. If no evidence of attracting sets or saddle points was found, the procedure was restarted with lower velocity limits. After having located a stable node, the usually present accompanying saddle was sought, being located within its local hyperbolic orbit segments by trial and error. The map was then re-started and the stable and unstable manifolds of the saddle were plotted, generally with the use of many interpolating orbits along the manifolds.

There are several practical difficulties inherent in manually plotting Poincaré maps. Firstly, motion along the stable and unstable manifolds is extremely rapid remote from the fixed point. Often only a small number of iterates will lie on the VDT screen. One is therefore forced to interpolate many intermediate orbits along these manifolds to obtain an accurate representation of their often highly convoluted shapes. Unfortunately, in almost all cases of interest, it is not possible to trace the manifolds in the remote regions. Rapid motion is exaggerated in systems with low coefficients of restitution and it proved possible to produce phase maps only for systems with $0{\cdot}8 \leqslant r \leqslant 0{\cdot}98$. Physically, for very inelastic systems, the "transients" die away after two or three impacts.

3.4. CLASSES OF "GENERIC" SYSTEMS

It is useful to divide the vibro-impact systems into four broad classes which show typical or generic types of behaviour. One can initially make the obvious division into preloaded and clearance systems, $(c = 0,\ \lambda > 0)$ and $(c \geqslant 0,\ \lambda = 0)$. According to the discussion of section 3.1, these can be further divided into sub-classes depending upon the ratio σ. In a clearance system, $\sigma = c/\beta = kc/F_0$ and the ratio compares the spring restoring force at impact to the excitation amplitude. Behaviour will obviously be highly dependent upon σ in the sense that if $\sigma > 1$ there will be braking forces at impact for any impact phase, whilst if $\sigma < 1$ the excitation can exceed the restoring force near impact phases of 0 or 2π. These considerations are useful but the material in section 3.1 actually shows that the regions of behavioural change—separated by a global bifurcation—are $\sigma \in]|\gamma|, |\sigma_*|[$ or $\sigma \in [0, |\gamma|[$. There are no single impact periodic points in $\sigma \geqslant \sigma_*$; any that did exist will be removed in a saddle-node bifurcation at $\sigma = \sigma_*$. In the interval $]|\gamma|, |\sigma_*|[$, a stable spiral node and a saddle-point can coexist. A global bifurcation must occur in this interval at the tangency of W^s and W^u of the saddle point. It will be seen that this will imply that the stable point will be a global attractor except for some initial conditions within the tangle. The saddle point disappears at $\sigma = |\gamma|$ and the remaining spiral sink becomes a true global attractor in $[0, |\gamma|[$. Of course, for frequency ratios where there are no fixed points, the behaviour is more complicated and will involve chaotic attractors and/or multiple impact subharmonic orbits. A parallel set of considerations apply to preloaded systems.

Basing one's classification on the intervals $|\gamma|$ and $|\sigma_*|$ complicates the picture because γ depends upon z and σ_* depends upon r, subharmonic number n, and z. For this reason the classes of behaviour will be divided roughly into the four categories $(c \geqslant 0,\ \lambda = 0,\ \sigma < 1)$, "large amplitude" clearance systems, $(c \geqslant 0,\ \lambda = 0,\ \sigma > 1)$, "low amplitude" clearance

systems, ($c=0$, $\lambda>0$, $\sigma<1$), "small preload" systems, and ($c=0$, $\lambda>0$, $\sigma>1$) "large preload" systems. The phase portraits typical of the above four crude classes will be discussed in turn.

3.5. PHASE PORTRAITS FOR CLEARANCE SYSTEMS

Perhaps the most important lesson learnt during this investigation is that chaotic responses are probably more likely (for a random initial condition) than periodic responses. For $\sigma>1$, large clearance or low amplitude, the chaotic motion will usually arise from motion following the stable manifold W^s outside the domain of attraction of a stable spiral single impact node past the saddle and then following the low velocity component W^u_- of the unstable manifold W^u which will usually wind rapidly about the cylindrical phase space and will either eventually become turbulent and become trapped by a chaotic attracting set or interact with some other fixed points at low velocity. These low velocity fixed points can be of the multiple impact type or single impact. They almost always involve homoclinic tangles. The simultaneous existence of two single impact fixed points is unusual and the lower sink usually corresponds to a conjugate pair of sink plus saddle for higher subharmonic number, the low velocity saddle point being past its homoclinic bifurcation. The chaotic wandering behaviour of W^u_- occurs when the manifold is ensnared by a low velocity attracting set and may seem completely random if few iterations are computed. However, if many thousands of iterations are computed, a more systematic picture of a one-dimensional strange attractor will usually emerge. Such simulations can take hours on a typical microcomputer and are best performed on a mainframe. If $\sigma<1$, corresponding to small clearance or large amplitude, the generic situation is that there is a large stable node whose domain of attraction is essentially the whole phase space. A saddle point will accompany the stable node at much lower velocity and the lower components W^s_- and W^u_- will be involved in a homoclinic tangle. The tangle is an external repellor and thus all external initial conditions will flow into the sink. Initial conditions above the saddle and between W^s_+ and W^u_+ will flow smoothly into the sink, but outside this region the tangle will introduce turbulence into any orbit that passes close by, perhaps capturing it for a few iterations before spitting it out. The orbit then winds with diminishing turbulence into the sink. Initial conditions within the tangle may eventually be rejected but others may evolve into almost periodic eddying orbits within the tangle, perhaps being involved with some of the strange invariant sets predicted by the Smale homoclinic theorem. Yet another way that chaos can occur is in the z-regions where no stable single impact orbit can exist. As z varies, one is either in a situation where the conjugate pair of stable node plus saddle point exists or where a single stable node exists. In the first region, variations in z will lead to a saddle node bifurcation: i.e., both fixed points must be destroyed simultaneously. However, in the second region the periodic orbit must disappear in a flip bifurcation to produce a saddle point with a double impact double period attractor. It is well known that in this z region further z-variations can lead to a finite or infinite cascade of period doubling bifurcations and the appearance of strange attractors. Previous authors [2] have presented examples for $c=0$. Analogous examples for $c>0$ will be presented here.

3.5.1. $\sigma<1$ *Or "high amplitude" behaviour*

The first example examined is a system with $c=0{\cdot}1$, $r=0{\cdot}98$, $\beta=0{\cdot}5$, $z=3{\cdot}7$ and therefore $\sigma=0{\cdot}2$. In this case, $|\gamma|\sim 0{\cdot}08$ and, after having observed that $n=2$ from the time series, $\sigma_*=3{\cdot}69$, from which it follows that $\sigma\in\,]|\gamma|,\sigma_*[$, so that the conjugate pair can exist. Figure 5(a) depicts the phase portrait in the region of the stable node on the cylindrical phase space Σ^+_c. The vertical axis is the velocity axis of the cylinder (with an

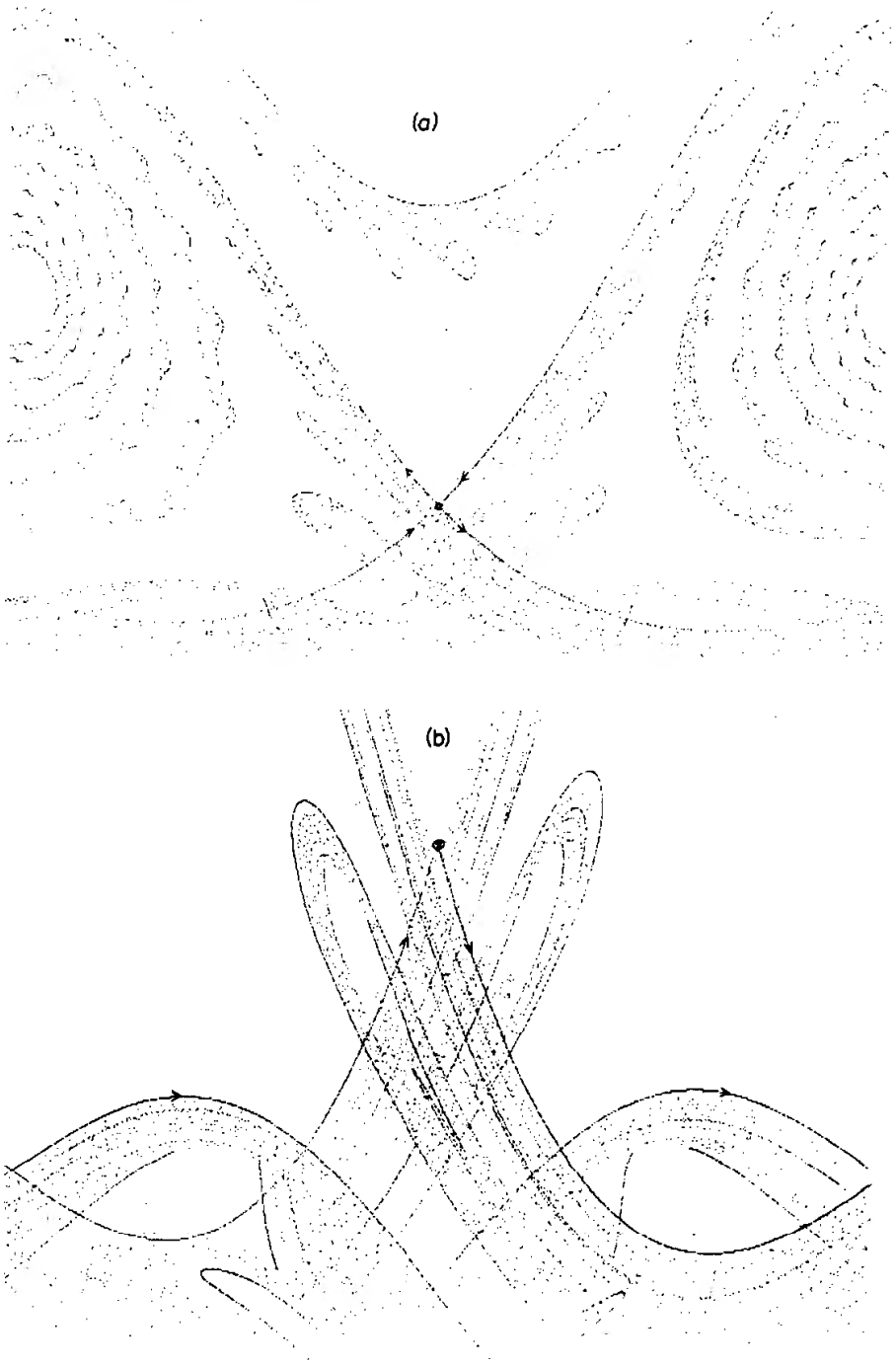

Figure 5. (a) High amplitude global attractor; (b) homoclinic tangle in Figure 5(a).

arbitrary convenient normalization) and the horizontal axis is the excitation phase $0 \leq \tau \leq 2\pi/z$. The left-hand vertical edge is to be identified with the right-hand edge to produce the cylinder. There are no attractors at higher velocities than those depicted.

A high velocity initial condition will at first flow gently (because $r \sim 1$) down the cylindrical phase space until it arrives in the region illustrated. Initial conditions entering on the right-hand side, in the region bounded by W^s_+ on the right and above the saddle point, will flow into the sink, experiencing transient chaos as they enter, due to the ripples impressed into W^u_+ by the homoclinic tangle. However, orbits that enter the region bounded by W^s_+ and W^u_+ will flow towards the tangle and experience severe transient chaos in the region of the tangle before being ejected and captured by the sink. Also illustrated in the figure is the way that W^u_- as well as W^u_+ is captured by the sink. In the former case, as implied by the λ-lemma, W^u_- accumulates along W^u with increasingly violent oscillations and is drawn into the node along with W^u_+. Similarly, W^s_- accumulates

along W^s_+ with violent oscillations eventually merging at infinity. Figure 5(b) depicts a more detailed view of the homoclinic tangle. It was produced by computing seven iterations from 3000 initial conditions on W^u_- and W^s_- close to the saddle point. The transverse intersections show up nicely although it is difficult to decipher any structure from the plot.

The next phase portraits trace the global bifurcation as σ is decreased and leads to a change in phase portrait from a pair of attracting sets to a single global attractor. Figure 6(a) depicts the phase portrait of a system with $c = 0{\cdot}1$, $r = 0{\cdot}98$, $z = 3{\cdot}7$ and $\beta = 0{\cdot}1$. The phase portrait is very clearly defined except at very low velocities, the stable and unstable manifolds of the saddle point being free of turbulence. The stable manifold W^s divides Σ^c_+ into two domains of attraction, that of the sink and that of a very low velocity attractor into which W^u_- smoothly spirals. Because relatively few high velocity initial conditions lie outside the wide spiralling domain of attraction of the sink, the probability of capture

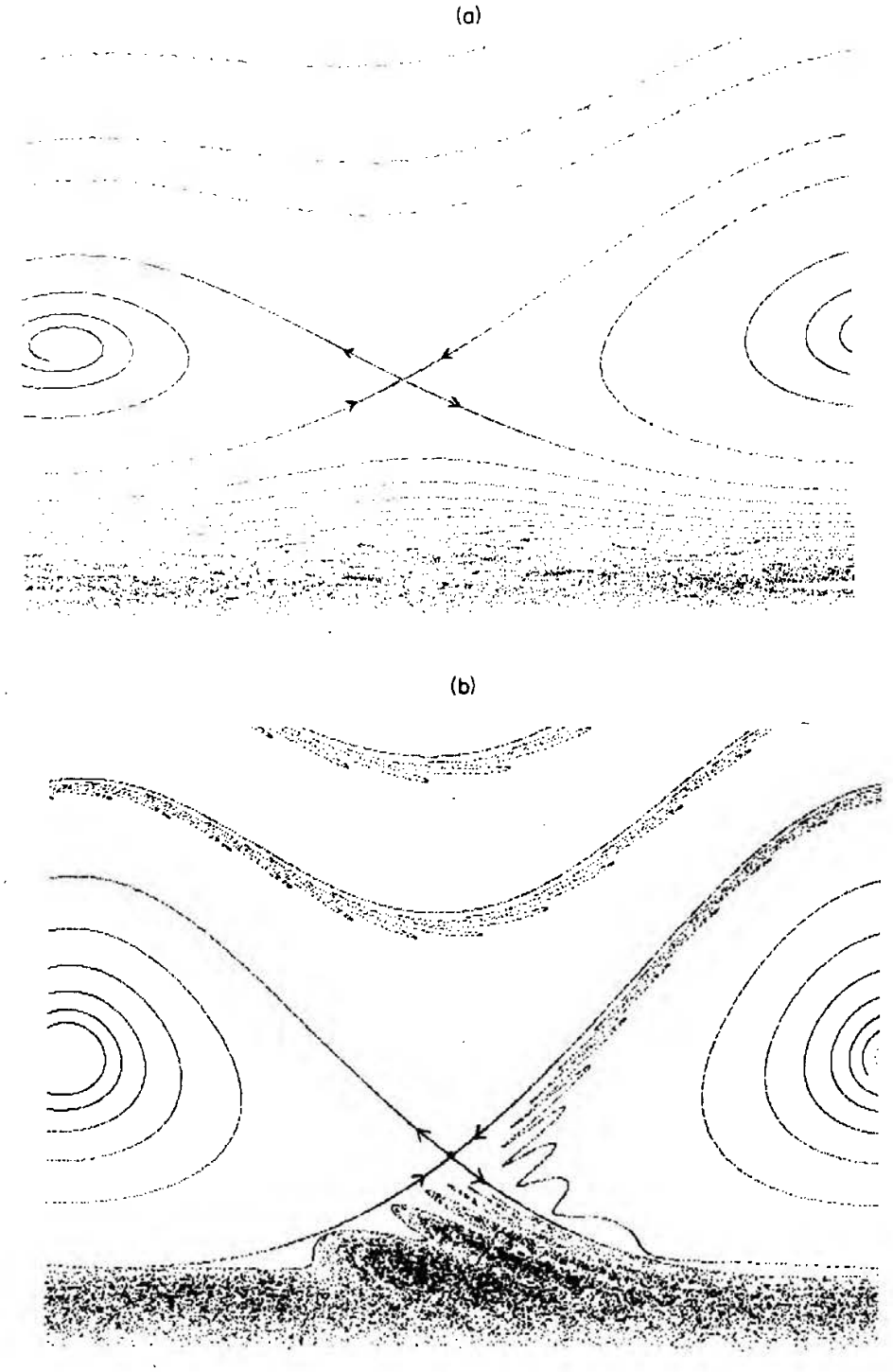

Figure 6. (a) Smooth winding of the stable manifolds in a low amplitude clearance system; (b) approach to tangency of the stable and unstable manifolds.

into the periodic point x at velocity greater than v_0, which is proportional to Area $(W^s(x) \cap \{v > v_0\})$, is high. As v drops below the stable velocity, the probability of capture by the sink falls to zero whilst the probability of capture by the low velocity attracting set (which is finite everywhere) increases to 1. Figure 6(b) depicts the effect of increasing the excitation amplitude. The phase portrait for $\beta = 0{\cdot}26$ shows that W^u has become extremely turbulent as it is drawn into the low velocity attractor which almost completely fills the region below the saddle point. A similar attractor corresponding to $\beta = 0{\cdot}25$ is depicted in Figure 7 and this appears to comprise a complicated one-dimensional Cantor manifold, the strands of which oscillate in a manner modelled by the function $\sin(1/x)$ towards W^u. A slight increase in β leads to a homoclinic global bifurcation where the low velocity attractor disappears, its oscillations now occurring in those of the homoclinic tangle as depicted in Figure 1(a), where the node has become a "global" attractor and the strange attractor has been replaced by a strange repellor. Thus, the homoclinic bifurcation has essentially involved a change in stability type of the low velocity attractor.

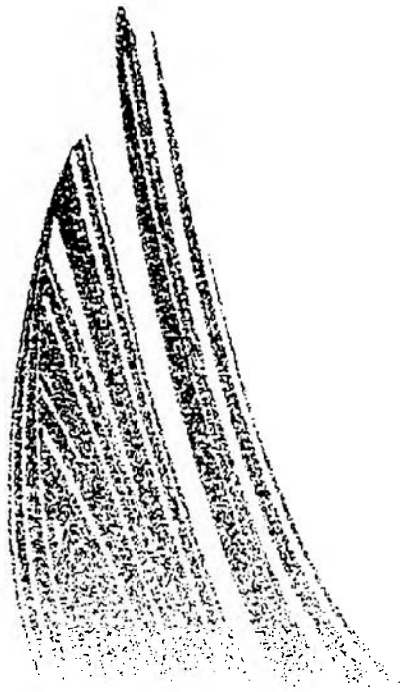

Figure 7. Low velocity strange attractor.

As amplitudes increase and σ decreases to $|\gamma|$, the saddle point must disappear, leaving only the stable point. An example of a phase portrait containing the stable point as a global attractor is shown in Figure 8. This is actually the superposition of many interpolated orbits. Turbulence seems to be generated in the orbits when they enter the neighbourhood of the grazing interval. One can visualize the flow as similar to the flow of a fluid against an obstruction along the grazing line with a stagnation point at the α point, turbulence being generated at impingement. Care should be exercised with this interpretation, however, because the flow is not continuous.

3.5.2. $\sigma > 1$ *Or low amplitude behaviour*

For low amplitudes compared to a given positive clearance, the situation is generically similar to that depicted in Figure 6(a) in parameter regions where single impact fixed points can exist. In this case, however, it is the low velocity region below the saddle point which exhibits the interesting behaviour. This behaviour is dictated by that of the unstable manifold W^u_-. In some cases, W^u_- will wind smoothly down the cylinder asymptoting to

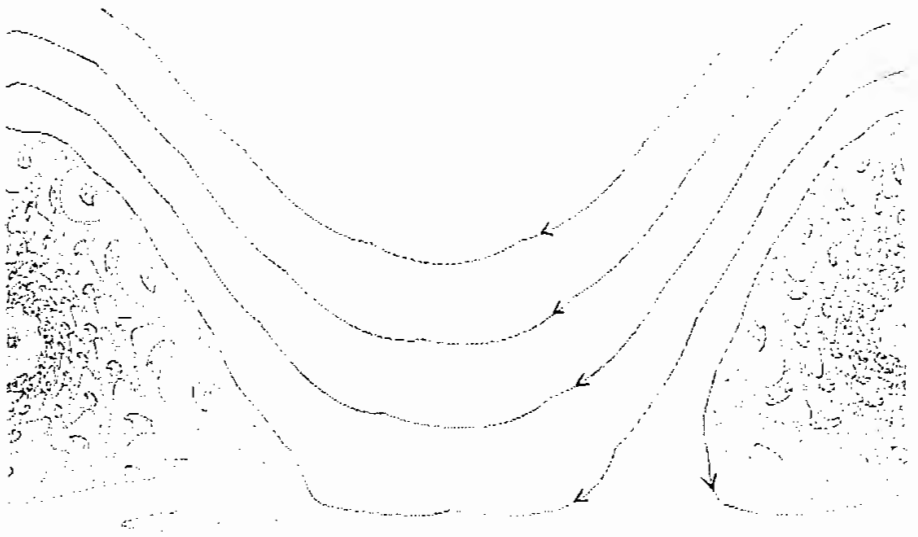

Figure 8. Turbulence induced by tangency.

$v = 0$, approaching itself arbitrarily closely. In mechanical terms, impacting just dies away but very slowly and at chaotic impact phases. The presence of low velocity attractors will usually imply an extremely complicated interaction between their stable manifolds and $W^u_\perp$. Indeed, the rapidity of motion makes any attempt to trace this interaction futile. If other stable fixed points exist in the low velocity regions they will usually be involved with saddle points with homoclinic tangles. Any such single impact fixed points will usually be of high subharmonic number. In this situation, multi-impact responses were frequently observed. Double impact stable motions comprising of a pair of spiral stable nodes with accompanying saddle points were common in some parameter ranges. For example, Figure 9(a) depicts a "high velocity" conjugate pair of stable node plus saddle point observed in a system with $c = 0{\cdot}4$, $\beta = 0{\cdot}05$, $r = 0{\cdot}98$ and $z = 3{\cdot}7$. In this system, $W^u_\perp$ spirals down the cylinder relatively smoothly until a pair of stable fixed points and associated saddles is encountered. Points flip from one sink to the other alternatively. The period 2 orbit is shown in more detail in Figure 9(b). Note the extremely complicated strange attractor.

In order to gain an insight into the nature of multiple impact orbits, it is useful to unroll the cylindrical phase space into its covering space, the upper half plane. The covering projection $R^+ \times R \to R^+ \times S^1$ is just $1 \times \pi$ where 1 is the identity map on R^+ and π is the covering map $R \to S^1$, $\tau \to |\tau| \bmod (2\pi/z)$. The Poincaré map $P: R^+ \times S^1 \to R^+ \times S^1$ used up till now is covered by $P_c: R^+ \times R \to R^+ \times R$ which forgets to reduce τ mod $(2\pi/z)$. These maps are all related by a commutative diagram:

$$\begin{array}{ccc} R^+ \times R & \xrightarrow[P_c]{} & R^+ \times R \\ 1 \times \pi \downarrow & & \downarrow 1 \times \pi. \\ R^+ \times S^1 & \xrightarrow{P} & R^+ \times S^1 \end{array}$$

P_c cannot have any fixed points because $P_c: (v, \tau) \to (v', \tau')$ with $\tau' > \tau$. A fixed point of P is covered by a fibre $(1 \times \pi)^{-1}(v, \pi(\tau)) = \{(v, \tau') \mid \tau' = \tau + 2\pi n/z\}$. The fibres are clearly invariant under P_c which acts as a time translation. Moreover, if the corresponding fixed point of P is a stable or unstable fixed point of period 1, its fibre is an attracting or repelling set for P_c. One can extend the unrolling technique to each orbit of P. In the present system, given a high enough initial velocity, the orbit will always wind monotonically down the cylinder due to energy losses at impact which cannot be replenished by the excitation during free flight. A smoothly descending orbit on $R^+ \times S^1$ will unwrap to

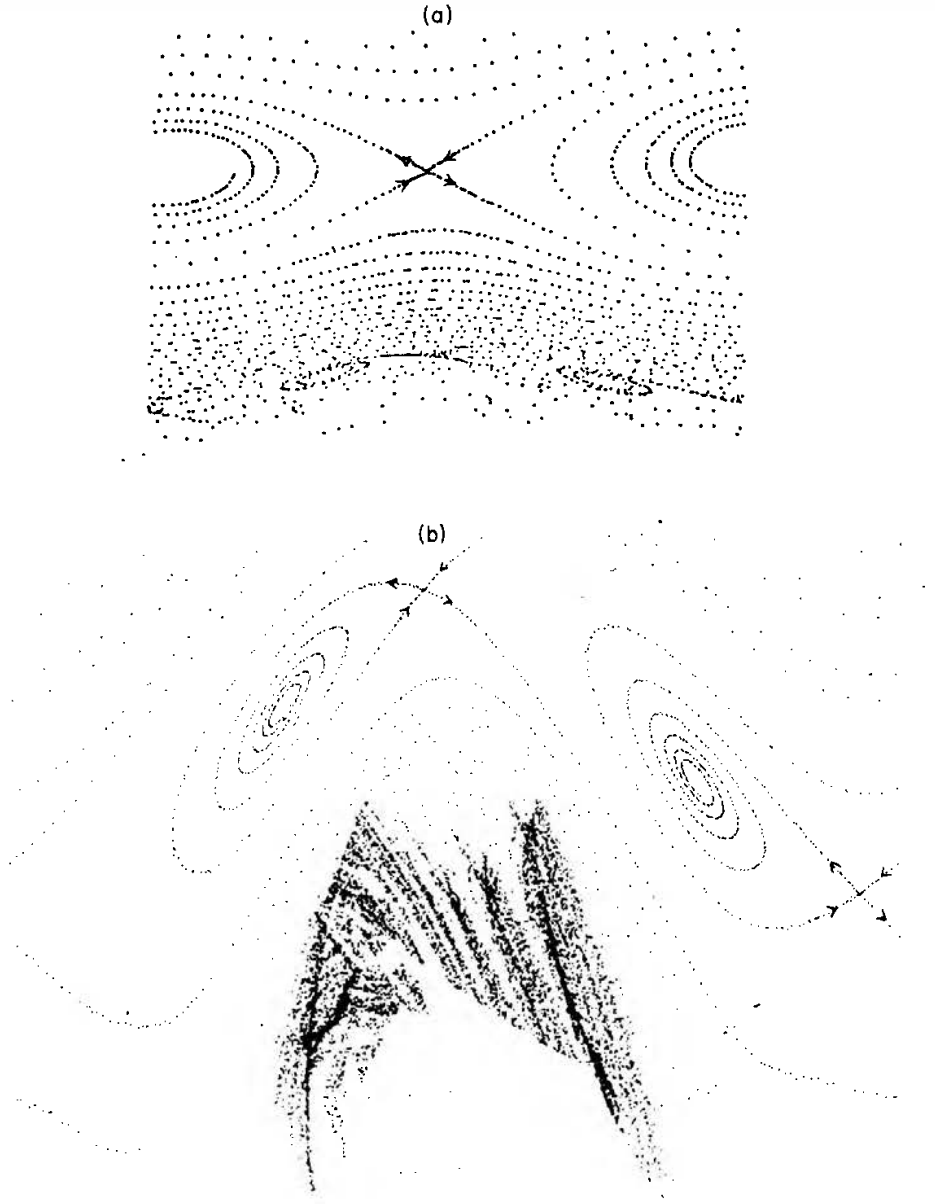

Figure 9. Coexistence of fixed points of orders 1 and 2; (b) detail of the period 2 fixed point.

a smoothly descending orbit of P_c on $R^+ \times R$. In the neighbourhood of an attracting set for P, the orbit of P_c will begin to oscillate as energy is gained and lost between impacts depending on impact velocity and excitation phase.

There are two possibilities. Either the oscillations die away as energy balance is approached or they persist. If they die away, a single impact orbit will result, each point of the orbit lying within a single fibre. If they do not die away, they either become periodic or aperiodic. Periodic oscillations represent multiple impact orbits, the multiplicity being the number of fibres visited. Aperiodic oscillations represent chaotic attractors. Figure 10 depicts unravelled orbits for a three impact per cycle orbit and a two impact per cycle orbit. In $R^+ \times S^1$ the points are visited cyclically, but in $R^+ \times R$ the points are visited in temporal sequence.

Multiple impact orbits were observed to be common for $z < 1$ but much less so for regions of $z > 1$ where stable single impact nodes were present. This is mechanically understandable in that for $z < 1$, the mechanical oscillator frequency ω_0 is higher than the excitation frequency. Thus there are many oscillator cycles per excitation period and hence more opportunities for multi-impact subharmonic cycles. The following examples were particularly clear cut. Figure 11(a) depicts a four-impact per cycle stable oscillation essentially comprising two saddle points of an unstable double impact pair following a

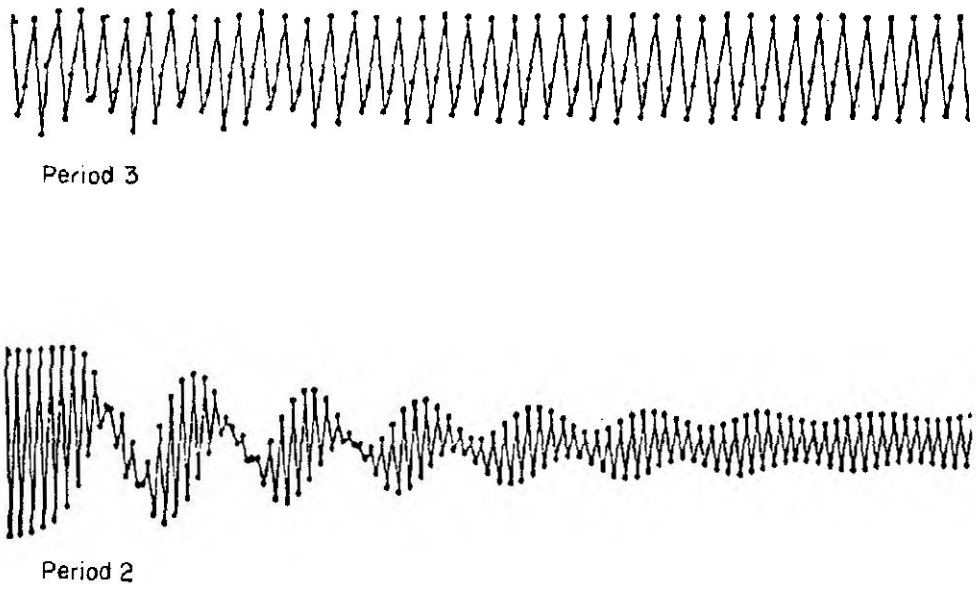

Figure 10. Orbit oscillations near fixed points of periods 2 and 3.

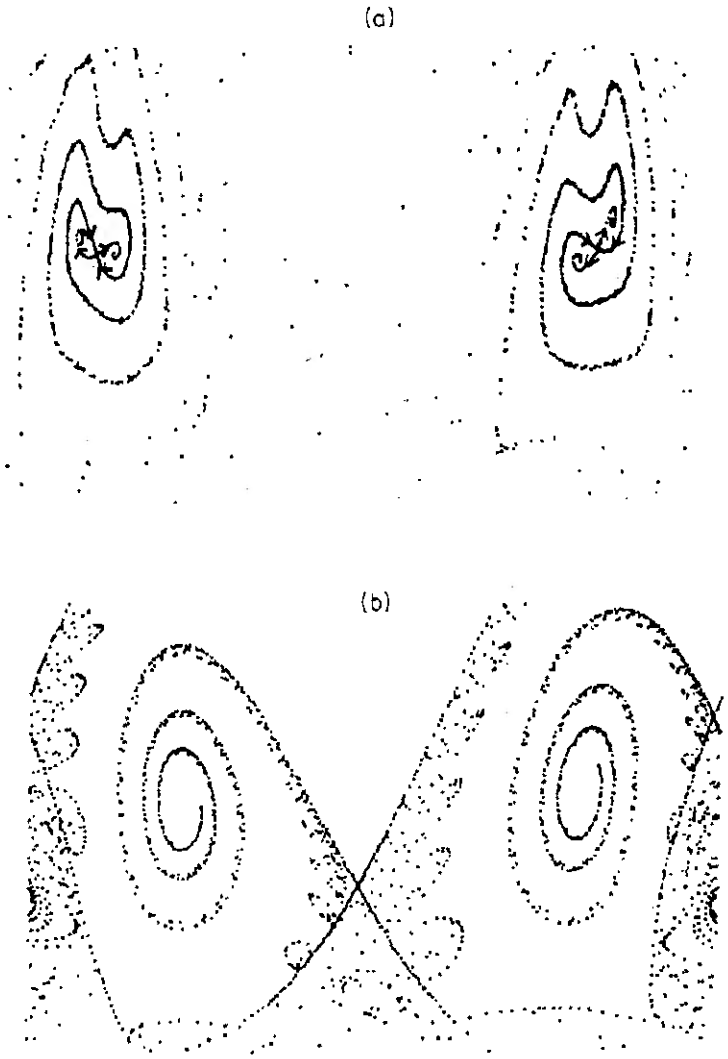

Figure 11. (a) Stable fixed point of order 4 after a flip bifurcation of a stable order 2 fixed point; (b) stable fixed point of order 2 with order 2 homoclinic tangle.

flip bifurcation, where the two saddles have both W^u_+ and W^u_- captured by a sink, each visited in a quartic cycle. The stable manifolds of both components wind into the saddles as fossils of a once stable pair of sinks. The parameters in this example are $r = 0{\cdot}98$, $\beta = 0{\cdot}2$, $c = 0{\cdot}1$ and $z = 0{\cdot}7$. Figure 11(b) depicts a double impact sink with a pair of asymmetric homoclinic tangles, one of which contains a stable fixed point of order 1. The period 2 orbit is globally attracting modulo the tangle. In this case, the parameters are $c = 0{\cdot}1$, $r = 0{\cdot}98$, $\beta = 0{\cdot}2$ and $z = 0{\cdot}9$.

It is of some interest to obtain the separatrices of the period 1, period 2 and chaotic attractor's domains of attraction for systems such as those in Figure 9(a). However, after numerous attempts, computer simulation yielded ambiguous results. The method adopted was to try to plot the unstable manifold W^u_- in the region of the period 2 attractor. Some orbits supposedly on W^u_- were captured by the period 2 attractor and some by the chaotic attractor. This may well have been caused by numerical errors. However, it may be the case that the stable manifold of the period 2 orbit winds very close to the high velocity saddle point. If so, the overall picture is of three separate spirally interwound domains of attraction on $R^+ \times S^1$ with the domain of the period 2 attractor becoming vanishingly thin at high velocities passing close to the right of the saddle and then expanding substantially in the intermediate region.

The next series of figures illustrates the saddle-node bifurcation as the clearance passes through σ_* for a system with $r = 0{\cdot}98$, $z = 3{\cdot}7$, $\beta = 0{\cdot}05$. Figures 12(a)-(c) are phase portraits plotted for $c = 0{\cdot}15$(a), $0{\cdot}182$(b) and $0{\cdot}185$(c). At $c = 0{\cdot}186$ there is only a kink in the flow of P in the region once occupied by the fixed points. With $n = 2$ (confirmed by plotting the time series), $\sigma_* = 3{\cdot}7036$ whilst for system (c), $\sigma = c/\beta = 0{\cdot}185/0{\cdot}05 = 3{\cdot}70$ in accordance with the theoretical calculation. Similar saddle-node bifurcations occur at the boundaries of stable motion in frequency ratio when the discriminant passes through zero. Saddle-node bifurcations were also observed in double impact systems where period 2 saddle-node bifurcations were observed, each saddle-node being visited cyclically.

Following the analysis of section 2, it is clear that for large clearances, the subspace N_c of non-impacting initial conditions becomes large. Thus only very violent initial conditions ever impact. Equally, below σ_* stable impact orbits that do exist will be at high impact velocity, $V_{n\pm}$ are roughly linear in σ below σ_*. If the orbit of the initial impact misses the domain of attraction of the single impact attractor one would expect the orbit to approach grazing in a geometric series as in the unexcited impact system for $\sigma \gg 1$. The latter condition ensures that the spring force at impact dwarfs the excitation force. Although this does occur for very low velocities, the situation turns out to be a little more complicated in practice.

Figure 13(a) depicts a phase portrait for a system with parameters $c = 0{\cdot}1$, $r = 0{\cdot}98$, $\beta = 0{\cdot}001$ and $z = 2{\cdot}2$, yielding $\sigma = 100$. The sink and saddle represent $n = 2$ stable and unstable subharmonic responses for which $\sigma_* = 193$. Note that the unstable manifold W^u_- of the saddle tangles into a chaotic attractor within which impacting occurs at an extremely low rate. For all intents and purposes impacting just stops. Figure 13(b) is plotted for a system with $x_c = 0{\cdot}1$, $r = 0{\cdot}9$, $\beta = 0{\cdot}05$, $z = 3{\cdot}0$ and therefore $\sigma = 2{\cdot}0$. This is an $n = 2$ response for which $\sigma_* = 4{\cdot}11$. In this case, W^u_- winds turbulently down the cylinder to eventually asymptote to grazing impact. Again impacting occurs at a very low rate at low velocities.

3.6. PHASE PORTRAITS FOR PRELOAD SYSTEMS

The purpose of this section is similar to that of the previous section, that is, to attempt to illustrate the generic behaviour of preloaded impacting systems. As in the above section, attention is restricted by practical considerations to almost elastic systems. The phase

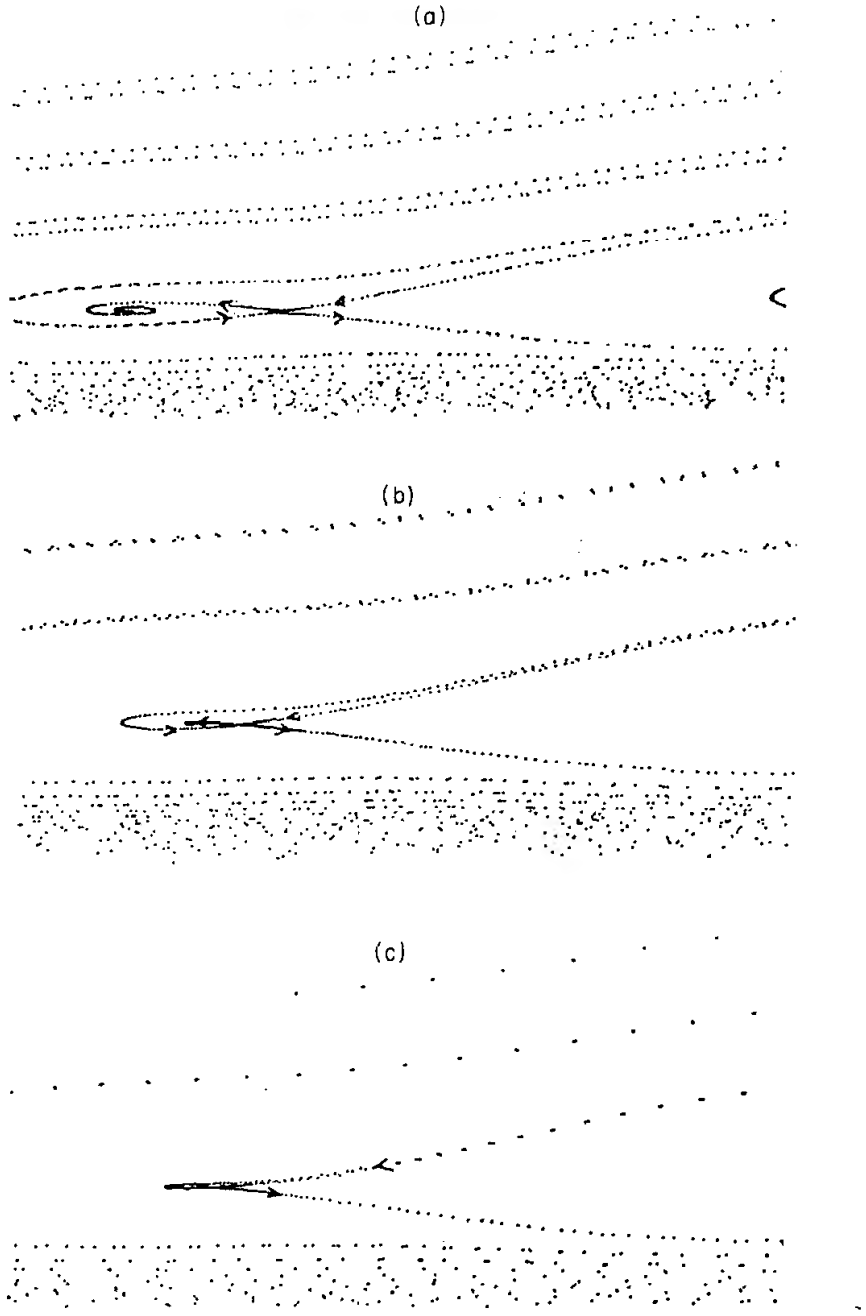

Figure 12. Occurrence of a saddle-node bifurcation in a clearance system as the clearance passes through the critical value. (a) $\sigma = 0{\cdot}15$; (*b*) $\sigma = 0{\cdot}182$; (*c*) $\sigma = 0{\cdot}185$.

portraits considered below are only for systems in parameter ranges allowing periodic motions. Preloaded systems ($c = 0$, $\lambda > 0$) will be split into lightly loaded, $\sigma = \lambda/\beta = N/F_0 < 1$, and highly loaded, $\sigma > 1$, although as mentioned above, it is more exact to split σ ranges into $]0, |\gamma|[$ and $]|\gamma|, \sigma_*[$, where the first interval can only contain a single stable period 1 fixed point whilst the second can contain a conjugate pair of period 1 fixed points. Recall from section 3.1 that $\sigma_*(n)$ is a maximum preload below which single impact subharmonic period n responses can exist and is a bifurcation point where the sink and saddle point mutually annihilate.

Lighly loaded systems will be discussed only briefly because they closely resemble the zero preload systems discussed in section 3.4. Most attention will be directed to the highly loaded systems because their phase portraits serve to illustrate the effect of trying to eliminate impacting in engineering systems where it can be a problem. Adding a preload to engineering systems prone to vibro-impacting is a well known remedy. It is applied, for example, to industrial heat exchangers with loosely supported tubing by adding spring

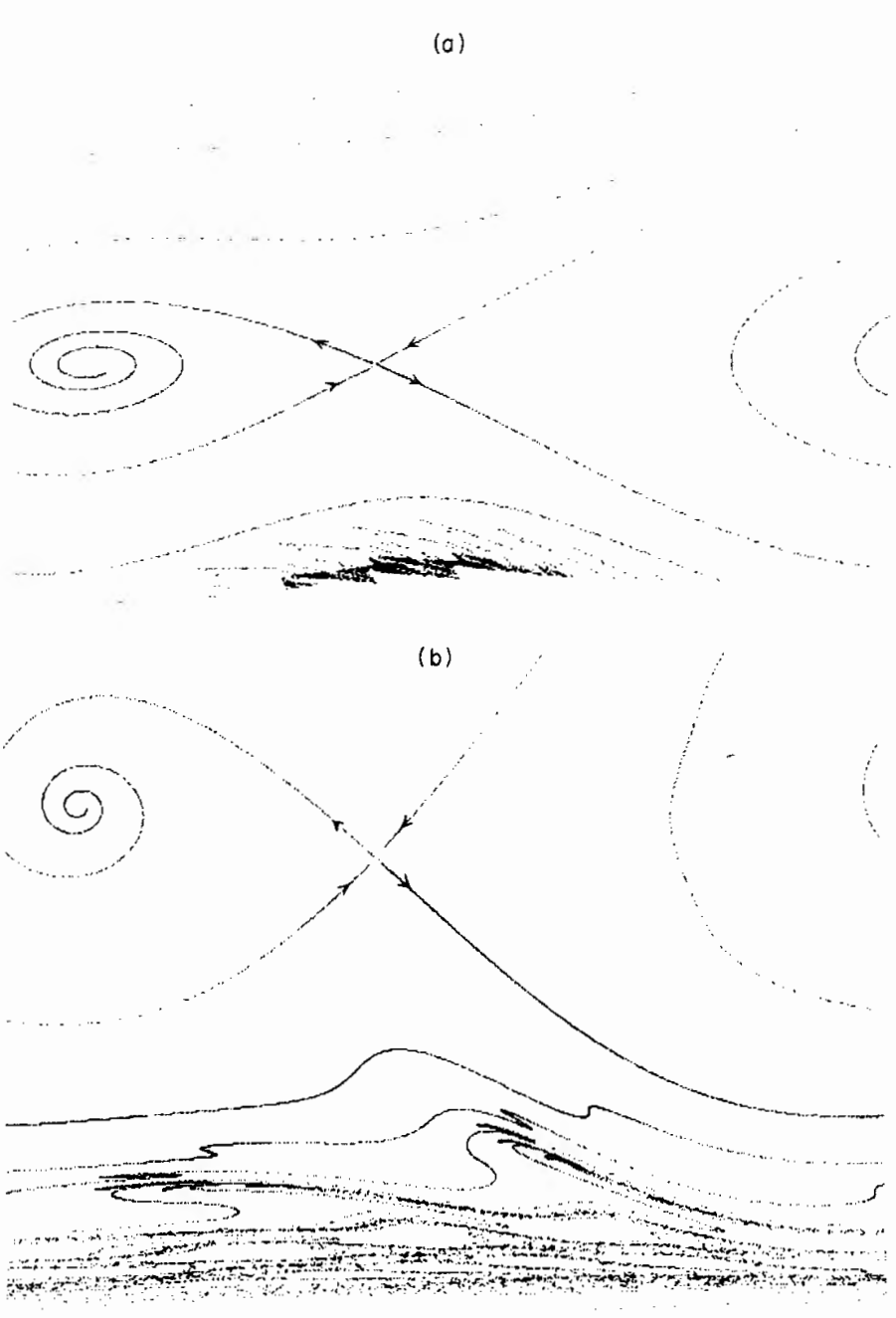

Figure 13. (a) Large clearance system with low impact rate low velocity terminal attractor; (b) large clearance system where impacting is asymptotic to grazing.

clips or antivibration bars to preload loose joints without locking them solid—they have to be free to slide under thermal expansion or contraction. Looseness is often also desirable in order to facilitate assembly.

It is clear from the earlier considerations that preloads below $\sigma_*(n)$ will not eliminate single impact, subharmonic order n, periodic response for all initial conditions. Because the stable impact velocity is approximately linear in preload below $\sigma_*(n)$ any periodic responses that remain will actually be more damaging at higher preloads. However two effects are improving the situation: (1) as σ increases, the domains of attraction of any stable fixed points become narrower—fewer high velocity initial conditions are trapped into stable vibro-impact; (2) as σ increases, any turbulence in the unstable manifold W^u_- of the associated unstable response becomes ironed out; this implies that low velocity attractors will die out; the terminal (static) attractor becomes the only asymptotic limit for low velocity orbits.

In any engineering system, it should be possible to estimate "worst case" initial conditions on Σ^+_c. In this way one could attempt to design a preload σ such that the

worst case initial condition is below the lower limit of the domain of attraction of any single impact fixed point. If the excitation is harmonic (or roughly harmonic) one can compute the frequency ratio z. Because subharmonic period n solutions only exist in the neighbourhood of $z = 2n$, one can estimate the nearest n that can occur and compute $\sigma_*(n)$. If this is impracticably high, calculation of V_{n+} will yield a "safe" upper velocity line, say $\{V_{n+}/2\} \times S^1$, below which impacting is killed by the preload. One would hope that one's "worst" initial condition lies in $v < V_{n+}/2$, otherwise stable impacting is probable. For harmonic excitation, one way to estimate the worst initial impact velocity is to calculate $\omega\gamma_0 F_0$ (the stable velocity for free (lightly damped) periodic response). For approximately harmonic excitation it would be appropriate to include an estimated crest factor in the excitation amplitude if RMS amplitudes are utilized. The problem of suppressing impact response by preloading is usually approached by simply assuming $N > F_0$: i.e., $\sigma > 1$ is safe. Clearly, this assumption is naive. It will serve only to prevent static initial conditions from impacting. Any transient in F_0 which reduces σ below 1 will initiate impacting from the rest condition. If crest factors in F_0 are taken into account, the above rule is effective. However, in any multicomponent system one cannot guarantee that design preloads will actually be implemented or remain constant if initially implemented properly. For example, transport of a system from the factory to the industrial location might well destroy any carefully designed preloading system. It is therefore wise to assume that a spectrum of preloads will exist and to attempt to assess the probability of damaging steady state motions in systems ranging from the design preload to clearance systems.

3.6.1. *Lighly loaded systems*

Lightly loaded, $\sigma = N/F_0 < 1$, vibro-impact systems are very similar to small clearance systems and therefore only one simulation will be discussed. Systems with a stable fixed point are represented by Figure 14(a) which is the phase portrait of a system with $\lambda = 0{\cdot}1$, $z = 2{\cdot}2$, $r = 0{\cdot}98$, $\beta = 0{\cdot}2$ and therefore $\sigma = 0{\cdot}5$. The immediately noticeable feature of this map and others for $\sigma \in]|\gamma|, \sigma_*[$ is that the saddle lies to the left of the sink. The pair sits at $(V_{n+}, \tau_n + \pi/z)$, (V_{n-}, τ_n) rather than at (V_{n+}, τ_n), $(V_{n-}, \tau_n + \pi/z)$ in clearance systems. The stable node is of the "global attractor" type with a homoclinic tangle in the unstable and stable manifolds of its conjugate saddle point. A more detailed view of the tangle is depicted in Figure 14(b) showing traversal intersections. A typical initial condition will undergo transient chaos before settling into steady state vibro-impact. For systems with $\sigma < |\gamma|$, there are globally attracting fixed points directly analogous to those of clearance systems.

3.6.2. *Highly preloaded systems*

Highly preloaded vibro-impact systems resemble large clearance systems in some ways, but in general, they exhibit less pathological behaviour. Any single impact attractors inhabit high velocity regions of phase space, as in the clearance systems, but the low velocity regions usually contain orbits which asymptote to the static terminal attractor in a reasonable way. High preload attractors seem to be sensitive to the coefficient of restitution, tending to disappear for moderate inelasticity. This is physically consistent in that the preload damps negative velocity excursions and extra damping at impact can only act in concert. In clearance systems, the excitation can reinforce negative velocity excursions and make up energy lost at impact, for suitable parameter values. In the present systems $\sigma > 1$ implies that $N > f_0|\cos(\omega t)|$ for all t.

Figures 15(a) and (b) are phase portraits obtained for preloaded systems in a parameter variation run, amplitude being varied for a system with $r = 0{\cdot}98$, $z = 2{\cdot}2$ and $\lambda = 0{\cdot}1$, the

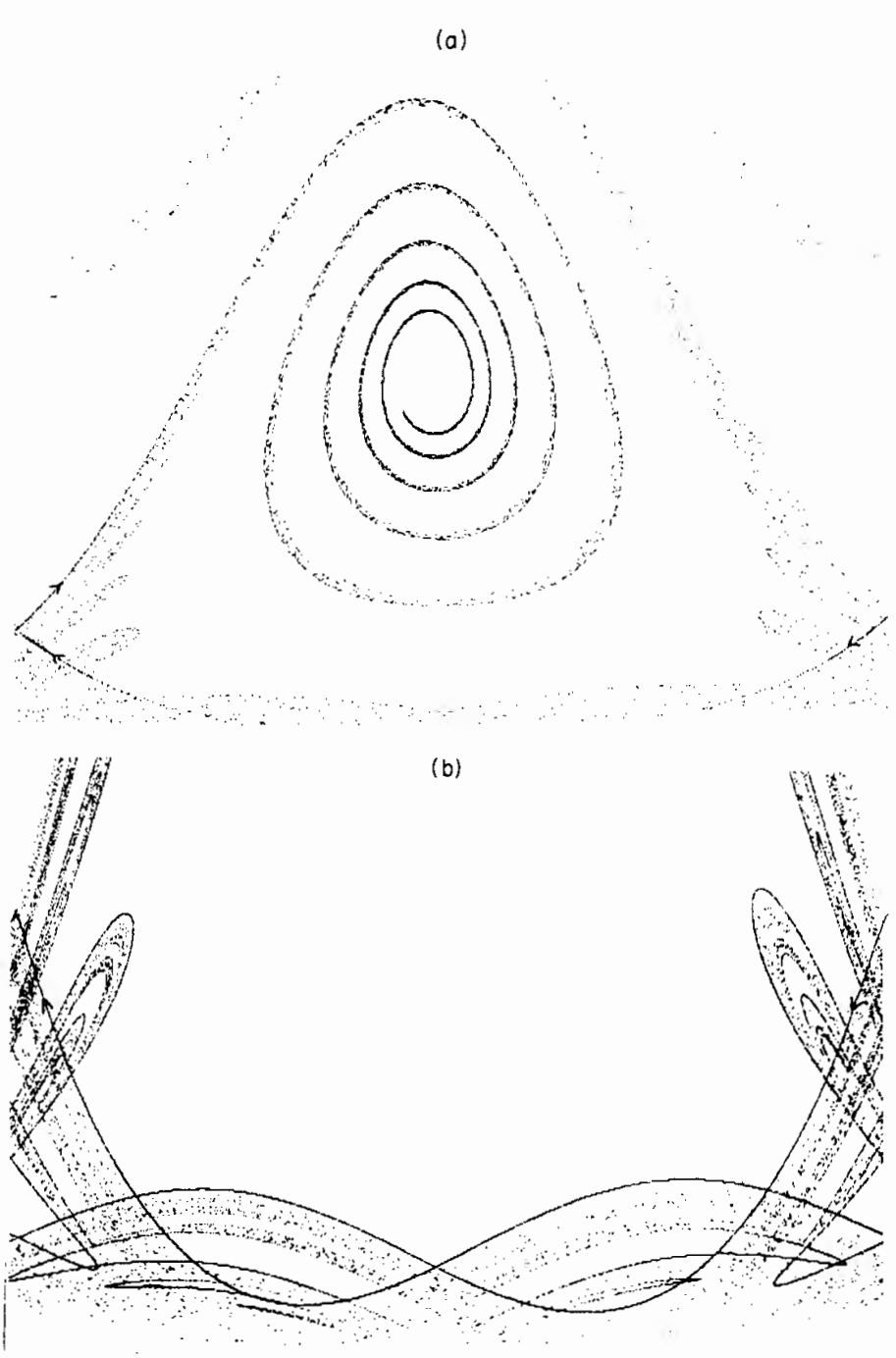

Figure 14. (a) Stable fixed point in a preload system with light loading showing a homoclinic tangle at the conjugate saddle point; (b) detail of the homoclinic tangle.

amplitude ratio β decreasing from 0·1 to 0·0125. The system in Figure 15(a) has $\beta = 0{\cdot}1$ and therefore $\sigma = 1$. The stable fixed point is not a global attractor since there are no transversal intersections of the stable and unstable manifolds of the conjugate saddle point. Note that the system is close to tangency and W^u_- has pronounced turbulence as has W^s_+. The stable fixed point is almost a "global" attractor for high velocity initial conditions because its domain of attraction almost fills the area above the saddle point. The initial conditions which are not trapped into stable periodic impacting become turbulent as they are dragged by the attracting unstable manifold W^u_- towards the terminal static attractor. As the excitation amplitude is reduced, the domain of attraction of the sink shrinks in area as the stable manifolds W^s_+ and W^s_- of the saddle move together. Almost all initial conditions are trapped by the static attractor. Decreasing the excitation amplitude also destroys the turbulence observed in the first phase portrait. Figure 15(b) is the phase portrait observed for $\beta = 0{\cdot}0125$ and hence $\sigma = 8$, and the system is clearly close to a saddle-node bifurcation. Plotting the time series of the stable fixed point yielded

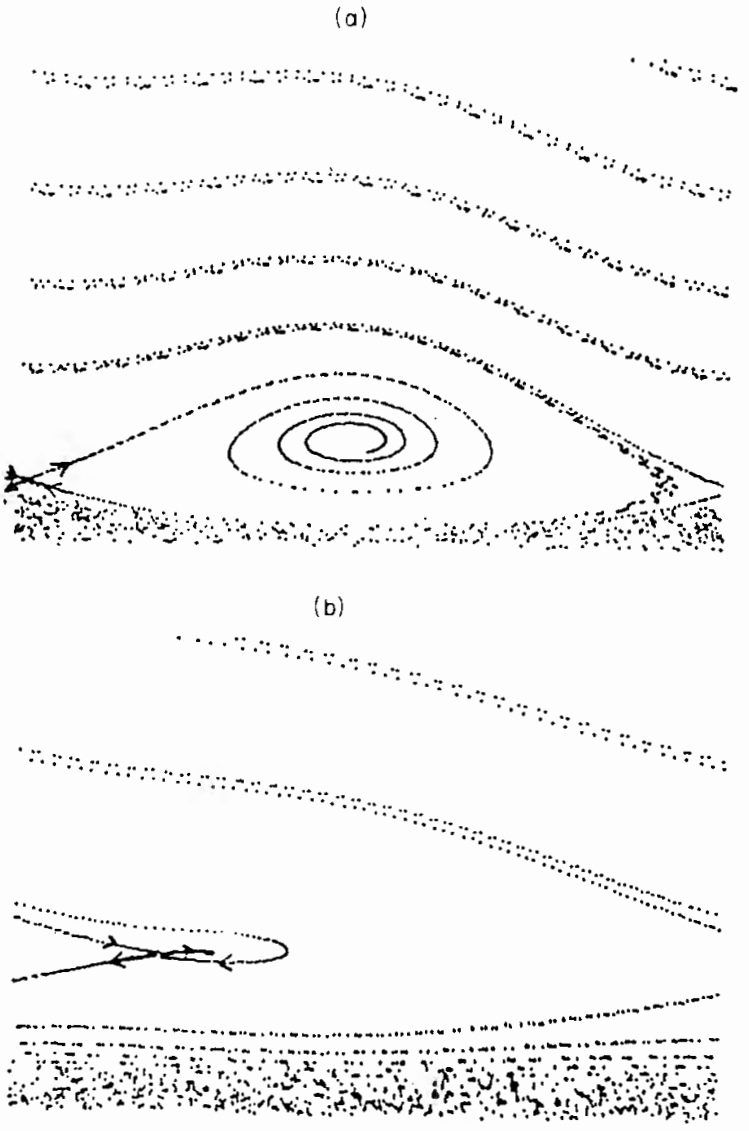

Figure 15. (a) Occurrence of a saddle-node in a preloaded system as the preload increases through the critical value σ_*; stable fixed point at $\sigma = 1$; (b) fixed point just before the bifurcation $\sigma = 8$.

$n = 1$. The critical ratio $\sigma_*(n)$ is 8·148. In this system, W^u_- spirals smoothly down to the static attractor approaching itself as it does so. Externally, this would appear as a terminal chaotic transient. This low velocity behaviour appears to be generic for high preload systems—and is clearly a desirable feature.

As mentioned above, the preload systems were found to be sensitive to the coefficient of restitution, stable fixed points existing only for $r \geq 0{\cdot}8$. In the system depicted in Figure 15(a), a saddle-node bifurcation erased the conjugate pair of nodes as r was decreased from 0·98 to just below 0·825 and $\sigma_*(n, z, r)$ decreased from 8·15 to 1·05. Similarly, a saddle-node bifurcation occurred when the frequency ratio was decreased from 2·2 to just below 2·05. Note that for $z = 2{\cdot}02$, $\sigma_*(n, z, r) = 1{\cdot}0606$. The conjugate pair persisted as z was increased past $z = 5$. Near $z = 3$, a homoclinic tangle was produced.

In systems with $z < 1$, multiple impact fixed points became relatively common, these being observed for $z > 1$ only as knots in tangles. For example, the system described above has an attracting double impact orbit in its tangle. Figure 16 depicts a nicely defined triple impact attractor in a system with $\lambda = 0{\cdot}1$, $r = 0{\cdot}98$, $\beta = 0{\cdot}1$ and $z = 0{\cdot}9$ which is not globally attracting. Most high velocity initial conditions and all low velocity conditions are trapped by the terminal attractor. Locking is approached with transient chaos as evidenced by the turbulence in the (3 component) unstable manifold of the attractor. This concludes the specific discussion of preloaded systems.

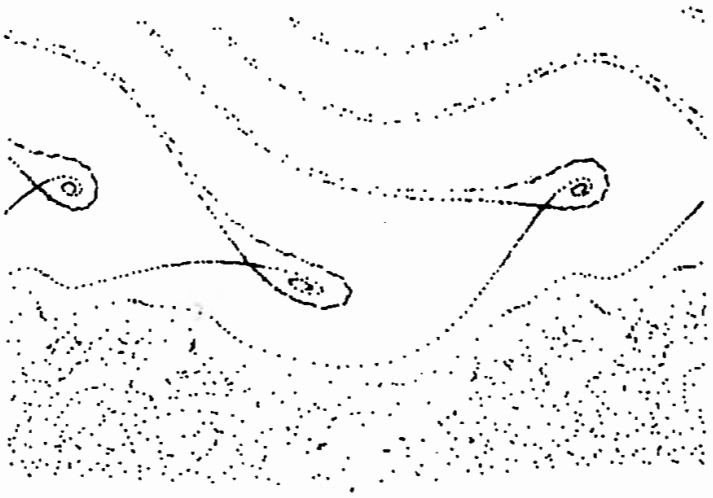

Figure 16. Triple impact attractor in a preload system showing turbulent unstable manifold.

3.7. SOME CHAOTIC ATTRACTORS

This section presents a discussion of chaotic attractors in the phase portraits of both clearance and preload vibro-impacting systems. The simulations described above produced several kinds of chaotic motions. Firstly, homoclinic tangles are present for "large" subspaces of parameter space and the tangles can cause transient chaos in local trajectories. Another type of transient chaos is produced in the neighbourhood of the grazing interval of phase space for systems with globally attracting fixed points.

Chaotic attracting sets are common in regions of parameter space where no stable fixed points exist. In the present systems, these regions are either those where a saddle-node bifurcation has occurred to annihilate a conjugate pair of single impact orbits or where a flip bifurcation has destabilized a stable node and created a pair of stable period 2 orbits. The flip bifurcation can cascade as a single parameter is varied and it is possible that such cascades are a necessary step in the lead up to a tangency of stable and unstable manifolds prior to transversal intersections and tangling. In reference [2] Shaw and Holmes demonstrated the existence of strange attractors for zero clearance systems in the latter unstable ranges for frequency ratios between the stable ranges for $n = 1$ and $n = 2$ single impact fixed points. Following a flip bifurcation at the $n = 1$ stability boundary, there is a cascade of flip bifurcations accumulating at $z = 2{\cdot}732$ for arbitrarily long period orbits. Taking account of these considerations, they observed a strange attractor at $z = 2{\cdot}8$ (for $r = 0{\cdot}8$). The strange attractor overlay the unstable manifold of the saddle point strongly suggesting coincidence.

A search was conducted in the present investigation for chaotic attractors of the above type in positive clearance and preload systems. Figure 17(a) depicts a chaotic attractor obtained in a positive clearance system with $c = 0{\cdot}1$, $r = 0{\cdot}7$, $\beta = 5{\cdot}0$ and $z = 2{\cdot}8$ and Figure 17(b) depicts a chaotic attractor in a preload system with $\lambda = 0{\cdot}1$, $r = 0{\cdot}9$, $\beta = 0{\cdot}9$ and $z = 1{\cdot}123$. The former simulation contains 5600 points plotted on a microcomputer and Figure 13(b) contains 30 000 points plotted by an IBM 4381. In the latter plot there are tangencies to the time axis near $\tau \sim \pi/2$ to which the orbit became trapped for many iterations—but it eventually escaped to produce the "well-defined" curve depicted.

Chaotic attracting sets are most commonly observed in the low velocity regions of large clearance or light preload systems and the attractor depicted in Figure 7 is a fairly typical example. It might be expected that they could be non-robust to system damping. This interesting question has not been investigated in the present study because high damping, small coefficient of restitution or viscous oscillator damping, gives rise to simulation difficulties. It should be mentioned that the latter damping mechanism was not investigated

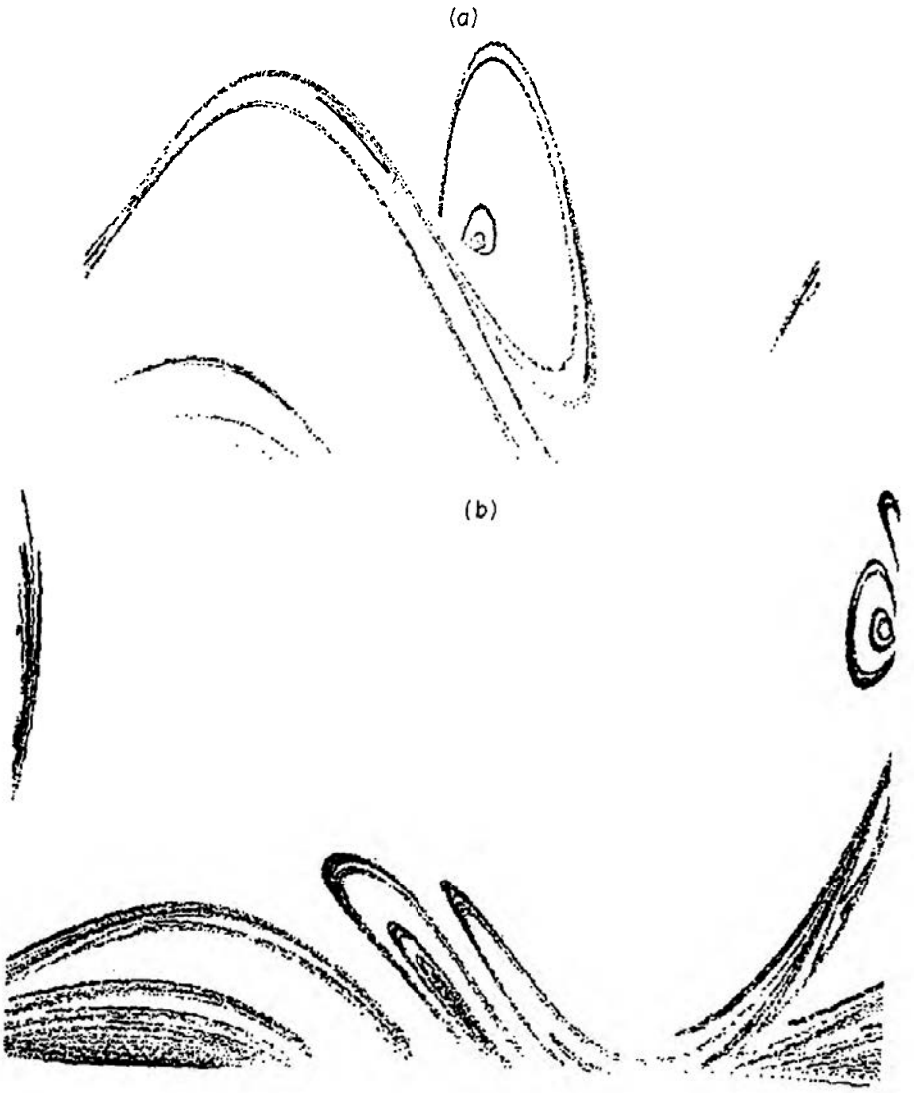

Figure 17. (a) Strange attractor observed in a positive clearance system, 5600 points on the orbit of a single point; (b) strange attractor observed in a preload system, 30 000 points on the orbit of a single point.

in the present study because it was felt that at levels of engineering interest ($\zeta \sim 0{\cdot}01$) the system should be structurally stable. However, this remains to be demonstrated.

This concludes the review of the phase portraits; in the next section an attempt is made at an overall appraisal of vibro-impacting systems and conclusions are drawn regarding the need for further work and the engineering consequences of the present investigations.

4. DISCUSSION

An exhaustive series of computer generated phase portraits of vibro-impacting dynamical systems have been constructed by using the Poincaré map, which samples the three-dimensional continuous orbits at the point of impact, producing a two-dimensional discrete dynamical system. It was not, of course, possible to scan the whole of the four-dimensional manifold of parameters corresponding to clearance (or preload), coefficient of restitution, frequency ratio and amplitude, but it is hoped that the systems considered were representative in the sense that most possible types of behaviour were observed, i.e., "most" C^0-equivalence classes were generated. In any case, passing from one class of system to another does involve a local or global bifurcation. It was possible to identify four classes of system in which "typical" phenomena occur. Roughly, these are ($c \geqslant 0$, $\lambda = 0$, $\sigma < 1$), ($c > 0$, $\lambda = 0$, $\sigma > 1$), ($c = 0$, $\lambda > 0$, $\sigma < 1$) and ($c = 0$, $\lambda > 0$, $\sigma > 1$). Passing from low amplitude to high amplitude involves a global homoclinic bifurcation

at the tangency of stable and unstable manifolds of a saddle point. A further bifurcation occurs as the latter saddle point crosses the time axis to vanish from the trajectory to convert the "almost global" attracting fixed point to a true global attractor. A further bifurcation occurs at the upper boundary of the C^0 class containing the conjugate pair of sink plus saddle which annihilates the latter fixed points. As well as the above easily noticeable bifurcations, it is probable that there can exist many more, less noticeable. For example, in some systems, low velocity stable periodic points (such as in Figure 9(a)) exist for some parameter values but not others. The broad bifurcation structure outlined above applies mainly to low amplitude clearance systems, large preload systems seem to be less complicated in many ways, possibly because of the high inherent "damping" supplied by the preload.

Whilst large regions of frequency ratio and preload/clearance space were explored, little investigation into the dynamics of highly inelastic ($r < 0{\cdot}8$) systems could be carried out due to computational difficulties with "high velocity" maps. Of course, the dynamics of single impact fixed points is amenable to algebraic analysis and thus local knowledge is directly obtainable. Nothing dramatically different occurs locally in such systems. However, one might expect the global behaviour to be rather different, especially in the large amplitude/low excitation clearance systems where much of the low velocity complex structure would probably be destroyed. It was observed in some preload systems that the coefficient of restitution could be a sensitive parameter. In this case it works in addition to the damping supplied by the preload. Decreases in the coefficient of restitution will rapidly narrow the regions where the conjugate pair of nodes exist because the critical ratio σ_* depends upon $(1-r)^{-1}$. Globally, increasing inelasticity will smooth out phase portraits. It may be that almost elastic impacts are the most interesting from an engineering point of view. The relative impact of two engineering structures will probably be almost elastic. Energy will be lost to friction involved in any sliding—some of which produces wear. Further energy losses occur by transmission of elastic waves, all of which may well be lost in exciting dissipative vibrations in other parts of the structure. The least applicable feature of the coefficient of restitution model is that real impacts are not instantaneous. For example, consider a pendulum which is rigid except for a hinge at some point which can impact a stop vertically above the static equilibrium position of the bob. On negative half cycles, the pendulum is "long" but as it swings back it is speeded up whilst the momentum of the bob pins the hinge against the stop until the pendulum again passes through its rest position. This type of impact lasts for an appreciable fraction of the vibration cycle and is representative of the impact of a beam against a stop. Shaw and Holmes discussed similar systems in reference [2], considering the impact of an oscillator on a spring, and Shaw and his co-workers used a similar approach in modelling the transverse impact of a beam at its tip as a 2 mode clamped (high frequency)—pinned (low frequency) system. Their analysis exhibited promising agreement with experiment [4, 5]. The instantaneous impact model is a first approximation to the impact of systems for which the impact duration is a small fraction of the system vibration periods. Its main usefulness is as an indicator of the phenomena which can occur in vibro-impact systems. The following paragraph constitute an attempt to summarize the engineering consequences of the work reported in this paper.

(1) The preloading of one-sided clearance interfaces between components in order to suppress impacting is useful only if it can be ensured that each interface is preloaded so as to exceed the maximum expected transient force amplitude. For a variety of reasons it is not practically possible to ensure that all interfaces are thus preloaded. In this case, there will be a spectrum of preloads down to zero preload and a spectrum of clearance gaps. At those positions where there is a gap or an inadequate preload, force transients

can initiate impacting. For large clearances or large preloads, violent initial conditions can lead to steady state impacting of either periodic type (possibly multi-impact per subharmonic cycle) or chaotic. It follows that inadequate preloading can actually exacerbate any vibro-impact problem in that it can induce more violent periodic impacting than would have occurred at zero clearance. This is because, when they exist, stable (single impact per subharmonic cycle) impact velocities increase roughly linearly with preload or clearance. It follows that a "little preload is a bad thing" and of course "that as high a preload as possible" is probably advisable.

(2) The considerations set out above apply only to "pinning down" the rest position. Once impacting under a preload has been initiated it can remain long after any generating transient has disappeared. Some of the material of section 3.5 will be re-iterated here. It is probably always possible to estimate what the largest possible velocity excursion might be. In this way, having a knowledge of the system parameters N (the design preload) r, z and β enables calculation to be made of the stable impacting velocity (if any) expected in the system. If the largest plausible initial impact velocity is below the stable velocity, then it follows that single impact per subharmonic cycle steady state response will not occur. Generically, one need only consider subharmonic numbers n "near" $z/2$. The possibility of chaotic steady state responses still exists, but for preload systems with $\sigma > 1$ these should not occur. (One should therefore choose a trial preload in this way—the philosophy of the approach of paragraph (1) above.) However, if the maximum expected initial impact velocity is above the computed stable velocity, there is danger of trapping into stable vibro-impacting, the probability being a function of the local relative area occupied by the domain of attraction—obtainable from simulations. In this case, the design preload is inadequate and it would be advisable to design to preloads above the bifurcation limit σ_* discussed in section 3.1. If $z < 1$ then, in general, there will be no single impact fixed points although multiple impact attractors may exist. At present, there are no quantitative methods available here and one would have to resort to numerical methods to determine the possibility of steady state impacting.

(3) A further use of the simple systems discussed in this paper is that they provide a conceptual model. Thus, in applying numerical techniques to more complicated structures, one has an idea of which parameters are likely to be sensitive and therefore important to get right and which are unimportant. Most engineering numerical simulations will consist of setting up a finite element model of a vibro-impact system, starting it off from rest and obtaining a long time series at huge CPU expense, and then drawing global conclusions about the system from the run. That this is probably a waste of time follows for several reasons. (i) Because simulations are expensive, only a small number of impact events is simulated; thus even if attractors do exist one may still be on a transient; the model behaviour may thus be totally unrepresentative of real phenomena. (ii) Impacting systems can exhibit extreme sensitivity to initial conditions and in any case, there are usually several attractors in phase space; different initial conditions can lead to completely different asymptotic behaviour; it is thus important to choose initial conditions representative of the real system under analysis. (iii) Impacting systems exhibit complicated bifurcation behaviour as parameters vary; a change of a few percent in a parameter can lead to totally different system responses. In numerical modelling one is in total ignorance of the bifurcation structure of the system of interest, any guesses as to the relevant parameters can thus lead to totally misleading answers. It follows from points (i)-(iii) that a numerical simulation is of any practical use only if many initial conditions are used for different parameter ranges and model structural variations. But this is just another way of constructing phase portraits. In fact, the only systematic approach is to use Poincaré mapping techniques—not necessarily strobing the impact velocity. For example, one could plot

displacement at a selected point, etc., at impact phase. Plotting phase portraits at various parameter values could indicate bifurcation behaviour and therefore parameter sensitivity. Previously, structural analysts have been content to produce vast time series files—Poincaré maps not only save disc space and listing paper; they also arrange the expensive computer data in a readable way. This technique also ought to be applied to the large numbers of experimental impact rigs in existence. Up till now, one extracted a time series of spiky output from one's rig, compared it with a spiky computer time series and concluded—they look similar—the model must be right!

(4) For clearance systems, one is in a similar situation as for preload systems in many ways. Small or zero clearances lead to steady state chaotic or periodic responses. As clearances increase, the impact velocities will also increase (at least for single impact periodic responses) until the stable motion disappears in a saddle-node bifurcation at the critical clearance σ_*. It follows that a little clearance is "bad" but a medium clearance is "worse".

(5) Further work is required in the following areas: (i) The global bifurcation in the present systems which occurs before the single impact saddle node crosses the time axis; (ii) simulation of the effect of $\alpha \to \omega$ trapping on the time axis should be carried out; Shaw and Holmes [2] have concluded that non-differentiable bifurcations occur via zero tangencies in zero clearance systems; further work should be carried out on such singularities; (iii) a classification of the homoclinic tangle beneath the saddle points of systems with $\sigma \in]|\gamma|, \sigma_*[$ would be of interest; (iv) A statistical analysis of chaotic attracting sets would be of some practical interest; for example, in plotting an attractor, one could simultaneously produce the probability distribution $\phi(v)$ of an impact with velocity in the range v to $v + \mathrm{d}v$; are these distributions in some sense universal in a C^0 stability class?; the curves could act as invariants if they were; they are of practical use in that impact wear depends upon impact force; impact wear is usually associated with a slide component at impact but, to a first approximation, one might only consider normal impact and estimate slide; impact velocity statistics would then convert to impact load statistics and allow estimation of wear rates through Archard's wear law; (v) More general impacting systems ought to be investigated, especially those involving two-dimensional impact/slide. In such systems, there are expected to be vast differences between systems with different impact boundary geometry. Different excitation forces are particularly relevant from a practical point of view; for example, industrial systems are usually subject to random excitation rather than harmonic. How can one gain impact statistics from excitation statistics? A family of systems of particular interest are the autonomous vibro-impactors; a self-excited oscillator can vibro-impact if its stable orbit intersects a line in phase space: can there be periodic solutions, chaotic attractors? Work of this type has been reported in reference [16]; (vi) Poincaré mapping techniques should be extended to the many large finite-element structural programs now in existence (see comment (1) above).

ACKNOWLEDGMENT

This work is published with the permission of the Central Electricity Generating Board.

REFERENCES

1. G. S. WHISTON 1987 *Journal of Sound and Vibration* **115**, 303–319. The vibro-impact response of a harmonically excited and preloaded one-dimensional linear oscillator.
2. S. W. SHAW and P. J. HOLMES 1983 *Journal of Sound and Vibration* **90**, 129–155. A periodically forced piecewise linear oscillator.

3. S. W. SHAW 1985 *American Society of Mechanical Engineers Journal of Applied Mechanics* 85-*APM*-14. Dynamics of a harmonically excited system having rigid amplitude constraints, Part 1—Subharmonic motions and local bifurcation.
4. S. W. SHAW 1985 *American Society of Mechanical Engineers Journal of Applied Mechanics* 85-*APM*-15. Dynamics of a harmonically excited system having rigid amplitude constraints, Part 2—Chaotic motions and global bifurcations.
5. S. W. SHAW 1985 *Journal of Sound and Vibration* **99**, 199–212. Forced vibrations of a beam with one sided amplitude constraint: theory and experiment.
6. S. W. SHAW and P. J. HOLMES 1983 *Journal of Applied Mechanics* **105**, 849–857. A periodically forced impact oscillator with large dissipation.
7. S. W. SHAW and F. C. MOON 1983 *International Journal of Non-Linear Mechanics* **18**, 465–477. Chaotic vibrations of a beam with non-linear boundary conditions.
8. J. GUCKENHEIMER and P. J. HOLMES 1986 in *Applied Mathematical Sciences* Series No. 42. Springer-Verlag, second edition. Non-linear oscillations, dynamical systems and bifurcations of vector fields.
9. D. R. J. CHILLINGWORTH 1976 *Differential Topology with A View to Applications.* London: Pitman.
10. R. H. ABRAHAM and C. D. SHAW 1983 *Dynamics—the Geometry of Behaviour, Part* 1—*Periodic Behaviour.* Santa Cruz: The Visual Mathematics Library, Ariel Press.
11. R. H. ABRAHAM and C. D. SHAW 1983 *Dynamics—the Geometry of Behaviour, Part* 2—*Chaotic Behaviour.* Santa Cruz: The Visual Mathematics Library, Ariel Press.
12. R. H. ABRAHAM and C. D. SHAW 1983 *Dynamics—the Geometry of Behaviour, Part* 3—*Global Behaviour.* Santa Cruz: The Visual Mathematics Library, Ariel Press.
13. S. NEWHOUSE 1980 in *Dynamical Systems: CIME Lectures Bressanone, Italy, June* 1978, *Progress in Mathematics No.* 8, 1–114: Birkhauser. Lectures on dynamical systems.
14. M. C. IRWIN 1980 *Smooth Dynamical Systems.* London: Academic Press.
15. G. S. WHISTON 1979 *Journal of Sound and Vibration* **67**, 179–186. Impacting under harmonic excitation.
16. D. K. ANDERSON 1985 *CEGB Internal Communication.* Steady state self-excited response of a symmetrically impacting single degree of freedom system.
17. G. S. WHISTON 1987 (to be published) Singularity structure in vibro-impact dynamics.